



Diabetic phenotype of transgenic pigs introduced by dominant-negative mutant hepatocyte nuclear factor 1 α



Kazuhiro Umeyama ^{a,b}, Masami Nakajima ^c, Takashi Yokoo ^d, Masaki Nagaya ^a, Hiroshi Nagashima ^{a,b,*}

^a Meiji University International Institute for Bio-Resource Research, 1-1-1 Higashimita, Tama-ku, Kawasaki 214-8571, Japan

^b Laboratory of Developmental Engineering, Department of Life Sciences, School of Agriculture, Meiji University, 1-1-1 Higashimita, Tama-ku, Kawasaki 214-8571, Japan

^c Department of Ophthalmology, Nihon University School of Medicine, 30-1 Oyaguchi, Kamicho, Itabashi-ku, Tokyo 173-8610, Japan

^d Division of Nephrology and Hypertension, Department of Internal Medicine, The Jikei University School of Medicine, 3-25-8 Nishishinbashi, Minato-ku, Tokyo 105-8461, Japan

ARTICLE INFO

Article history:

Received 23 September 2016

Received in revised form 5 December 2016

Accepted 31 January 2017

Available online 13 February 2017

Keywords:

Transgenic pig

HNF1 α (hepatocyte nuclear factor 1 α)

Dominant-negative mutant

MODY3 (maturity-onset diabetes of the young type 3)

Diabetic retinopathy

Diabetic nephropathy

ABSTRACT

Aim: The present study aimed to identify the characteristics of genetically modified pigs carrying a mutant human gene as a research model for diabetes and its complications.

Methods: We developed a transgenic cloned pig (founder, male) carrying a mutant gene, i.e., human HNF-1 α (P291fsinsC), which is responsible for maturity-onset diabetes of the young type 3. Transgenic progeny obtained via the artificial insemination of wild type (WT) sows with the cryopreserved sperm derived from the founder pig was pathologically examined.

Results: The transgenic progeny maintained a high blood glucose level (>200 mg/dL). Additionally, the oral glucose tolerance test results showed that the recovery of blood glucose levels in the transgenic progeny was significantly delayed compared with that in the WT semi-siblings. Hypoplasia of the islets of Langerhans was confirmed by the histopathological image of the pancreas, based on the hyperglycemia noted in the progeny being ascribed to decreased insulin secretion. Retinal hemorrhage and cotton-wool spots, i.e., findings consistent with non-proliferative diabetic retinopathy, were detected, and these progressed over time. The histopathological image of the renal glomeruli showed a nodular lesion that is characteristic of diabetic nephropathy in humans.

Conclusions: These data demonstrated that the genetically modified pig that we developed is a promising model for research on diabetes and its complications.

© 2017 The Authors. Published by Elsevier Inc. This is an open access article under the CC BY-NC-ND license (<http://creativecommons.org/licenses/by-nc-nd/4.0/>).

1. Introduction

Because pigs have many points of similarity with humans in terms of physiology and anatomy, they are frequently used in medical research as large experimental animals that can provide findings applicable to humans by extrapolation. In recent years, the production and use of disease model pigs in particular have been gaining attention.^{17,18} Similar to humans, pigs are (1) omnivorous; (2) likely to be obese; and (3) likely to be dyslipoproteinemic—similar humans with diabetes mellitus (DM) type 2—when they eat a high-fat diet.^{5,9} Hence, production of a porcine DM model is likely to contribute substantially to studies on the treatment of human DM and on measures related to complications of human DM.

Currently, three different methods are used to produce DM model pigs. One is chemical induction of DM, in which administration of a toxic glucose analog, such as alloxan or streptozotocin, is used to destroy pancreatic β -cells.¹⁶ However, this method is not practical

because of its poor reproducibility.¹⁴ Another method is surgical extirpation of the pancreas.²⁹ However, it is very difficult to obtain many individual animals for a study because extirpation of the pancreas requires high-level techniques and strict postoperative management.^{29,30} The third method uses genetic engineering. Methods generally used for production of genetically modified animals are transfer of a foreign gene to zygotes or somatic cell nuclear transfer using genetically modified cells.^{25,26,34}

We generated transgenic (tg) cloned pigs carrying the causal gene of maturity-onset diabetes of the young type 3 (MODY3).^{32,34} MODY3, a disease inherited in an autosomal dominant pattern, is induced by mutation of a transcription factor, hepatocyte nuclear factor 1 α (HNF1 α), and is characterized by dysfunction and attrition of pancreatic β -cells.^{1,6} The tg cloned pigs expressing the mutant HNF1 α showed constitutive symptoms of hyperglycemia since 2 weeks of age. Thus, the expression of the mutant HNF1 α was proved to cause MODY3 in pigs. The diabetic phenotype exhibited by the cloned pigs, however, was assumed to be influenced by the epigenetic modifications that are typically noted in cloned animals.^{31,34} Therefore, we grew one of the founder tg cloned pigs

* Corresponding author. Tel.: +81 44 934 7824; fax: +81 44 934 7824.

E-mail address: hngas@meiji.ac.jp (H. Nagashima).

obtained to sexual maturity by continuously administering insulin, and then collected its spermatozoa to produce progeny.³² Because the epigenetic status of the progeny obtained by sexual reproduction is normalized,³⁸ the phenotype of the progeny is likely to truly reflect the expression of the transferred gene, i.e., the mutant HNF1 α .

This study aimed to identify, in detail, the characteristic symptoms of DM in the progeny of a founder cloned pig with a mutant HNF1 α gene. Analysis of physiological characteristics, including blood glucose measurement and growth and blood biochemical properties, of the homo-father semi-siblings revealed that the mutant HNF1 α tg pigs are a strain showing typical clinical findings of DM. It was also revealed that these porcine phenotypes manifest the major complications of DM, confirming their potential value as a model of DM.

2. Materials and methods

2.1. Animals

The Institutional Animal Care and Use Committee of Meiji University approved all animal experiments in this study (IACUC 09-0006). All animal care and experimental procedures were performed in accordance with the regulations contained in the Japanese Act on Welfare and Management of Animals.

Wild-type (WT) and DM progeny from a tg cloned boar, a pig that developed DM (DM pig)—in which an expression vector carrying the human HNF1 α dominant-negative mutant P291fsinsC was integrated in a site on the long arm of chromosome 4³³—were used in the study. Briefly, spermatozoa were collected from a mutant HNF1 α tg cloned boar and were cryopreserved, as described in our previous report.³² These spermatozoa were used for in vitro fertilization (IVF) or intrafallopian insemination (IFI) to produce 16 animals that were used in our experiments between 0 and 12 months of age. All of the piglets produced underwent PCR-based evaluation for the presence or absence of the transgene,³⁶ and were subsequently classified as DM or WT pigs. Pigs were housed in a temperature-controlled room, had free access to water, and were provided with commercial feed appropriate to their growth-stage (Chubushiryo Co., Ltd. Nagoya, Japan) in accordance with the Japanese Feeding Standard for Swine.²¹ Body weights were regularly measured.

2.2. Biochemical analysis of plasma components

Changes in blood glucose levels and blood biochemistry of five DM pigs and eight WT pigs were followed up until the age of 4 months. Blood glucose levels were measured once a week from 2 to 17 weeks of age. Blood was obtained by ear vein puncture. Blood glucose was measured using a glucose test meter (GLUCOCARD GT-1820, Arkray Inc., Kyoto, Japan). In addition, blood biochemistry tests were performed once every month. Venous blood samples were collected in tubes containing heparin to determine the concentrations of aspartate aminotransferase (AST), alanine aminotransferase (ALT), blood urea nitrogen (BUN), creatinine, glucose, total protein, and potassium using a dry-chemistry analyzer (FUJI DRI-CHEM 7000, FUJIFILM Co., Tokyo, Japan). The concentration of 1,5-anhydroglucitol (1,5-AG) was determined using an enzymatic method (SRL, Inc., Tokyo, Japan). The concentrations of insulin-like growth factor-1 (IGF-1) were determined using an IGF-1 enzyme-linked immunosorbent assay (ELISA) (Mediagnost, Reutlingen, Germany).

2.3. Measurement of insulin secretory activity

Changes in blood glucose and insulin levels due to feeding were monitored in 5-week-old pigs. Blood samples of three DM pigs and four WT pigs were collected from the jugular vein before and after their feeding in the morning. After the initial blood collection, the animals were fed, and blood samples were collected again 45–50 min

after they started feeding. In order to perform an ELISA for insulin, aprotinin (Wako pure chemical industries, Ltd., Osaka, Japan) was added to venous blood samples at a final concentration of 200 KIU/mL (KIU: kallikrein inhibitor unit). The concentrations of insulin were determined using the Pig Insulin ELISA KIT (TMB) (Shibayagi CO. Ltd., Gunma, Japan) and the Mercodia Porcine Insulin ELISA (Mercodia AB, Uppsala, Sweden).

2.4. Oral glucose tolerance test

An oral glucose tolerance test (OGTT) was performed using three DM pigs and three WT pigs at 6 weeks of age. After fasting for 16 h, a glucose solution (3 g/kg body weight) was administrated to each pig through an oral catheter. Blood was obtained from the ear vein, and the blood glucose level was measured using a glucose test meter at 0, 60, 120, and 180 min after glucose loading.

2.5. Ophthalmoscopic examination of the eye fundus

Fundoscopy was performed in three DM pigs under general anesthesia using a mixture of sevoflurane (Pfizer Japan Inc., Tokyo, Japan), oxygen, and nitrogen monoxide. To achieve mydriasis, a mydriatic agent (Mydrin-P, Santen Pharmaceutical Co., Ltd., Osaka, Japan) was instilled into the eye of each pig. The fundus of each pig was examined using an indirect ophthalmoscope (HEINE OMEGA 500, HEINE Optotechnik, Herrsching, Germany) with a +28 diopter lens and was photographed using a fundus camera (GENESIS-D, Kowa Co., Ltd., Nagoya, Japan). For any individual with a progressed cataract, fundoscopy was conducted after removing the clouded lens by phacoemulsification using OS3 (Ophthalmic Small Incision Surgery System, Oertli Instrumente AG, Berneck, Switzerland) under general anesthesia.

2.6. Histochemical analysis and immunohistochemical analysis

Three DM pigs and five WT pigs were sacrificed by exsanguination under anesthesia at 4.5 months of age. Dissected organs were fixed in a 10% neutral-buffer formalin solution; embedded in paraffin; sectioned; and finally examined after hematoxylin and eosin (HE), periodic acid-Schiff (PAS), periodic acid-methenamine-silver (PAM), and Congo-red staining had been performed. For immunohistochemistry, pancreatic sections were incubated with diluted primary anti-insulin polyclonal guinea pig antibody (#N1542, Dako, Glostrup, Denmark) for 30 min at room temperature, followed by incubation with the secondary antibody of EnVision + Rabbit/HRP (#K4002, Dako) for 30 min, and finally stained with diaminobenzidine (#K3466, Dako). As a negative control, only secondary antibodies were applied.

2.7. Statistical analysis

Values for body weight and the biochemical parameters of the blood plasma were expressed as mean \pm standard error (SE). Statistical analyses were performed using SPSS 16.0 software (SPSS, Chicago, IL, USA). Differences were analyzed using a two-tailed Student's *t* test. *P* < 0.05 was considered statistically significant.

3. Results

3.1. Physiological/histological characteristics of DM pigs

Comparing the growth between DM and WT pigs, no difference in body weight gain was observed from birth until 5 weeks of age. However, weight gain in the DM pigs was attenuated from 6 to 17 weeks of age, which resulted in a significantly lower body weight as measured each week, compared with the WT pigs (Fig. 1A).

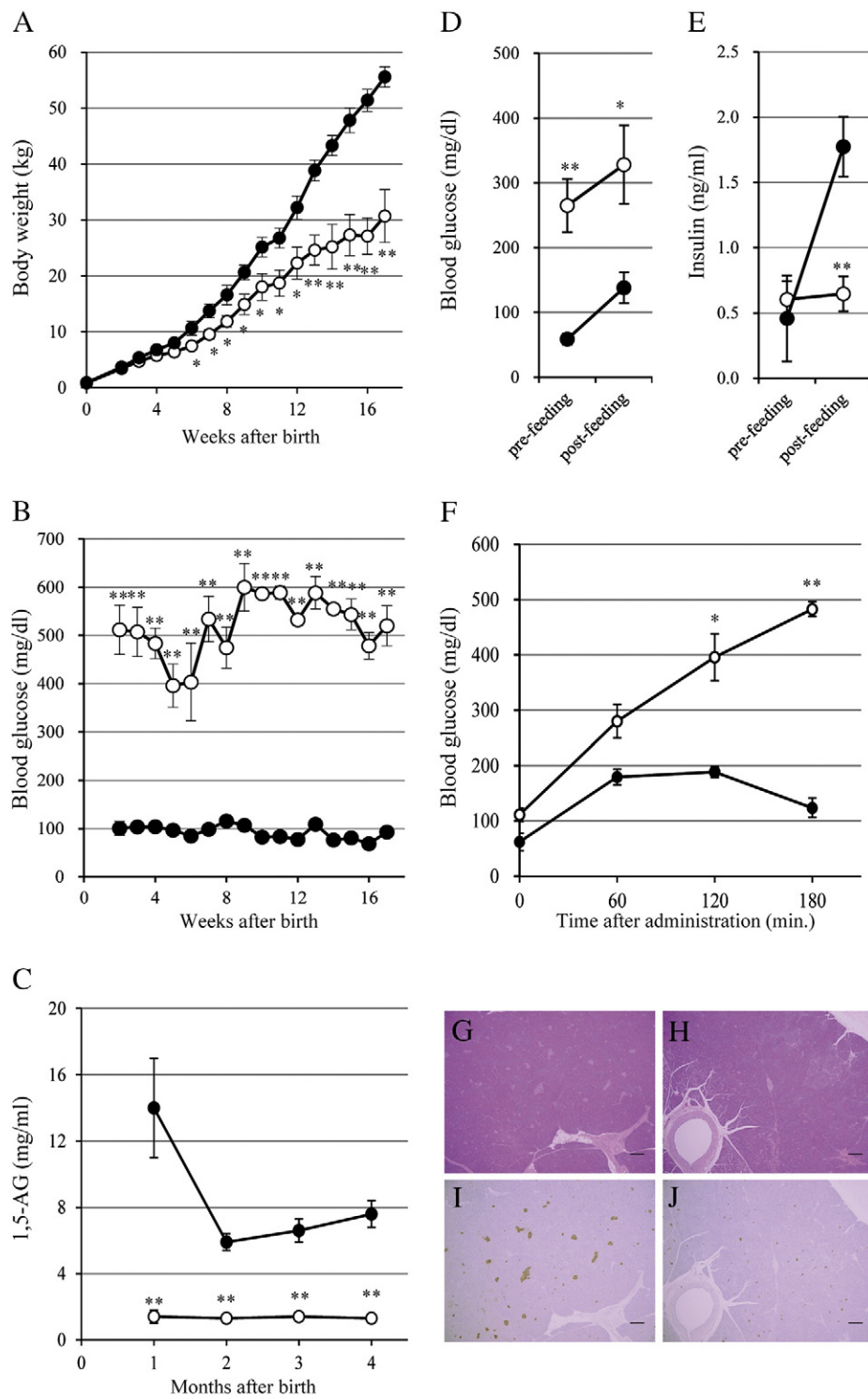


Fig. 1. Physiological and histological features of the mutant HNF1 α transgenic pigs. (A) Body weights of the WT (filled circles, $n = 8$) and DM (open circles, $n = 5$) pigs. (B) Non-fasting blood glucose concentrations of the WT (filled circles, $n = 8$) and DM (open circles, $n = 5$) pigs. (C) The plasma levels of 1,5-anhydroglucitol (1,5-AG) of the WT (filled circles, $n = 8$) and the DM (open circles, $n = 5$) pigs. (D) Changes in the preprandial and postprandial blood glucose concentrations. Filled and open circles indicate the WT ($n = 4$) and DM ($n = 3$) pigs, respectively. (E) Changes in the preprandial and postprandial insulin concentration in plasma. Filled and open circles indicate the WT ($n = 4$) and DM ($n = 3$) pigs, respectively. (F) Oral glucose tolerance test of the WT (filled circles, $n = 3$) and DM (open circles, $n = 3$) pigs. (G–J) Histopathological analysis of the pancreas. Paraffin-embedded sections from the WT (G and I) and DM (H and J) pigs were stained with hematoxylin and eosin (G and H) and with an antibody against insulin (I and J). Quantitative data shown are presented as the mean \pm SE. * $P < 0.05$, ** $P < 0.01$. WT, wild type; DM, diabetes mellitus.

The non-fasting blood glucose level of DM pigs was already higher than that of WT pigs when measurement commenced, at 2 weeks of age (512 ± 50.9 mg/dL vs. 101 ± 4.3 , $P < 0.05$). Thereafter, the level in DM pigs remained within the range of 396–600 mg/dL until 17 weeks of age, which was significantly higher ($P < 0.05$) than that of the WT pigs (69–116 mg/dL) (Fig. 1B).

The 1,5-AG levels measured in WT pigs were 15.1 ± 2.9 , 5.9 ± 0.5 , 5.9 ± 0.7 , and 7.6 ± 0.8 mg/mL at 1, 2, 3, and 4 months of age, respectively. In contrast, the levels measured in DM pigs were significantly ($P < 0.05$) lower and remained within a range of 1.3–1.4 mg/mL from 1 to 4 months of age (Fig. 1C).

Fig. 1(D and E) shows the results of an investigation of postprandial excursions in blood glucose and plasma insulin levels at 5 weeks of age. Compared with WT pigs, DM pigs showed significantly higher preprandial blood glucose levels (265 ± 41.0 vs. 59 ± 8.7 mg/dL, $P < 0.05$). However, no significant difference was detected in blood insulin levels at this time point between the groups. The subsequent measurement of the postprandial blood glucose level, which was conducted 45–50 min after the animals began eating, showed similar elevations in the WT and DM pigs. At this time point, WT pigs showed an elevation of the blood insulin level (from 0.46 ± 0.33 ng/mL to 1.77 ± 0.23 ng/mL), whereas DM pigs showed little elevation in the blood insulin level (from 0.60 ± 0.14 ng/mL to 0.65 ± 0.13 ng/mL). In the OGTT, the blood glucose level of WT pigs recovered to normal 180 min after the glucose load, whereas that of DM pigs remained high (**Fig. 1F**).

Fig. 1(G–J) shows the histology of the pancreas of DM and WT pigs. In the pancreatic tissue of DM pigs, β -cells stained by anti-insulin antibody were present in a scattered manner, and no clear Langerhans islets were seen (**Fig. 1H and J**), unlike the specimens from WT pigs (**Fig. 1G and I**). However, no morphological abnormality was found in the acinar tissue around the Langerhans islets, even in DM pigs (**Fig. 1H and J**). These results demonstrated that DM pigs show symptoms of DM due to a remarkable lowering of insulin secretion that is caused by a decrease in the number of β -cells in the pancreas.

3.2. Pathological findings in DM pig eyes

Cataracts began appearing in the eyes of DM pigs at approximately 2 months of age. At 4.5 months of age, clouding of the lenses was visually apparent (**Fig. 2A and B**). In the histopathologic examination of the lenses of 4.5-month-old DM pigs, vacuolization of the lens fiber in the equatorial region of the lens (**Fig. 2D**) and swelling of the lens fibers in the posterior pole of lens were observed (**Fig. 2F**). In addition, nucleated cells were found in the posterior pole of the lens in some DM pigs (**Fig. 2F**). The retinas of three DM pigs were subjected to repeated fundoscopy. From 4 months of age, retinal hemorrhage and cotton-wool spots, which are early symptoms of diabetic retinopathy—developed in all three animals (**Fig. 2G**). The disease progressed with time, and the number of cotton-wool spots observed at 5 months of age was greater than that at 4 months (**Fig. 2H**). At 12 months of age, vitreous hemorrhage—a clinical finding indicative of proliferative diabetic retinopathy—was observed in one of the three DM pigs (**Fig. 2I**). Moreover, a neovascular membrane-like finding was observed in the same individual (**Fig. 2J**).

3.3. Pathological findings in DM pig kidneys

Diabetic retinopathy is a condition detected in all patients with DM type 1 complicated by diabetic nephropathy. In patients with DM type 2, diabetic retinopathy is not always detected simultaneously with diabetic nephropathy.³ To clarify whether diabetic retinopathy and diabetic nephropathy developed simultaneously in our DM pigs, kidney tissues of three DM pigs were analyzed histopathologically at 4.5 months of age, after detection of their diabetic retinopathy at 4 months of age. In the renal glomeruli of all DM pigs, nodular lesions with mesangial matrix accumulations were identified (**Fig. 3B and D**). These lesions were not identified in WT pigs of the same age (**Fig. 3A and C**). The nodular lesions of DM pigs were negative for Congo red staining used to detect amyloid deposition. Therefore, the nodular lesions found in DM pigs were not amyloid deposits.

3.4. Blood biochemistry data

Fig. 4 shows the changes in blood biochemistry values of DM and WT pigs from 1 to 4 months of age. The BUN levels of DM pigs tended to be higher than those of WT pigs throughout the measurement

period, although they were within the normal range (10–30 mg/dL,¹² **Fig. 4B**). The CRE level (**Fig. 4C**) and K level (**Fig. 4D**) of DM pigs were also normal throughout the measurement period. These findings demonstrated that the kidneys were able to maintain normal blood biochemistry levels despite features of a diabetic nephropathy-like condition detected on histology at 4.5 months of age.

The AST (**Fig. 4E**) and ALT (**Fig. 4F**) levels of DM pigs were high at 2 months of age and were significantly higher than those of WT pigs at 4 months of age. The plasma level of insulin-like growth factor-1 (IGF-1) of DM pigs was constantly and significantly lower than that of WT pigs (**Fig. 4G**).

4. Discussion

In this article, we described the phenotypes of DM pigs expressing the mutant HNF1 α gene, particularly focusing on complications. Diabetic retinopathy and nephropathy are the most frequently seen microvascular disorders arising from DM. Diabetic retinopathy is staged based on its severity as simple diabetic retinopathy, non-proliferative diabetic retinopathy, and proliferative diabetic retinopathy.⁴ Many animal models of diabetic retinopathy have been generated, but no reported model to date has shown progression of the disease similar to that seen in humans.¹³ The symptoms manifested by the existing models are limited to early symptoms or proliferative angiogenesis in the last stage of diabetic retinopathy, thus making their application to human patients via extrapolation difficult.¹³ In the DM pigs that we developed, hemorrhage and cotton-wool spots, i.e., findings consistent with non-proliferative diabetic retinopathy, were detected at 4 months of age, and the conditions progressed over time. At 12 months of age, a neovascular membrane-like clinical finding—indicative of proliferative diabetic retinopathy such as vitreous hemorrhage and proliferative angiogenesis—was also detected. As the trajectory of symptom development is similar to clinical findings in human diabetic retinopathy, the pigs we developed seem to offer promise as a diabetic retinopathy model. In the future, analyses using techniques such as fluorescein angiography will further elucidate the characteristics of retinopathy in the DM pigs.

Cataract is another serious complication of DM.²³ In a hyperglycemic state, glucose that is not metabolized by hexokinase in the lens enters the polyol pathway, consisting of aldose reductase and sorbitol dehydrogenase, to be metabolized to fructose via sorbitol.²⁷ Sorbitol, a polar substance, cannot pass through the plasma membrane easily. Therefore, as the amount of glucose entering the polyol pathway increases, the accumulation of intracellular sorbitol increases, thus causing a hyperosmotic condition and/or water influx, leading to swelling of lens fibers and to changes in the permeability of the plasma membrane and the loss of intracellular substances, ultimately resulting in opacification of the lens.²⁷ In the porcine lens, aldose reductase, but not sorbitol dehydrogenase, is present,³⁵ indicating the absence of a metabolic pathway from sorbitol to fructose. Therefore, continuance of a hyperglycemic state is likely to cause an accumulation of sorbitol in the porcine lens. This is speculated to be the reason for the early development of diabetic cataracts in DM pigs.

Diabetic nephropathy is a serious primary disease that leads to end-stage kidney failure.² An animal model developing a renal disease similar to human diabetic nephropathy is useful for elucidating of the cause of, and the developing of novel treatments for, diabetic nephropathy.² A histological characteristic of human diabetic nephropathy is the presence of nodular lesions in the glomeruli, i.e., nodule-like structures that are formed by mesangial matrix expansion. Clinical symptoms of diabetic nephropathy are related to changes in the glomerular structure, particularly the degree of mesangial expansion.⁷ However, among the many DM mouse models that have been generated, only limited strains show nodular lesions.^{8,11,39} Moreover, there is no reported diabetic model of pigs developing nodular lesion-like renal lesions.²⁵ In contrast, in the DM

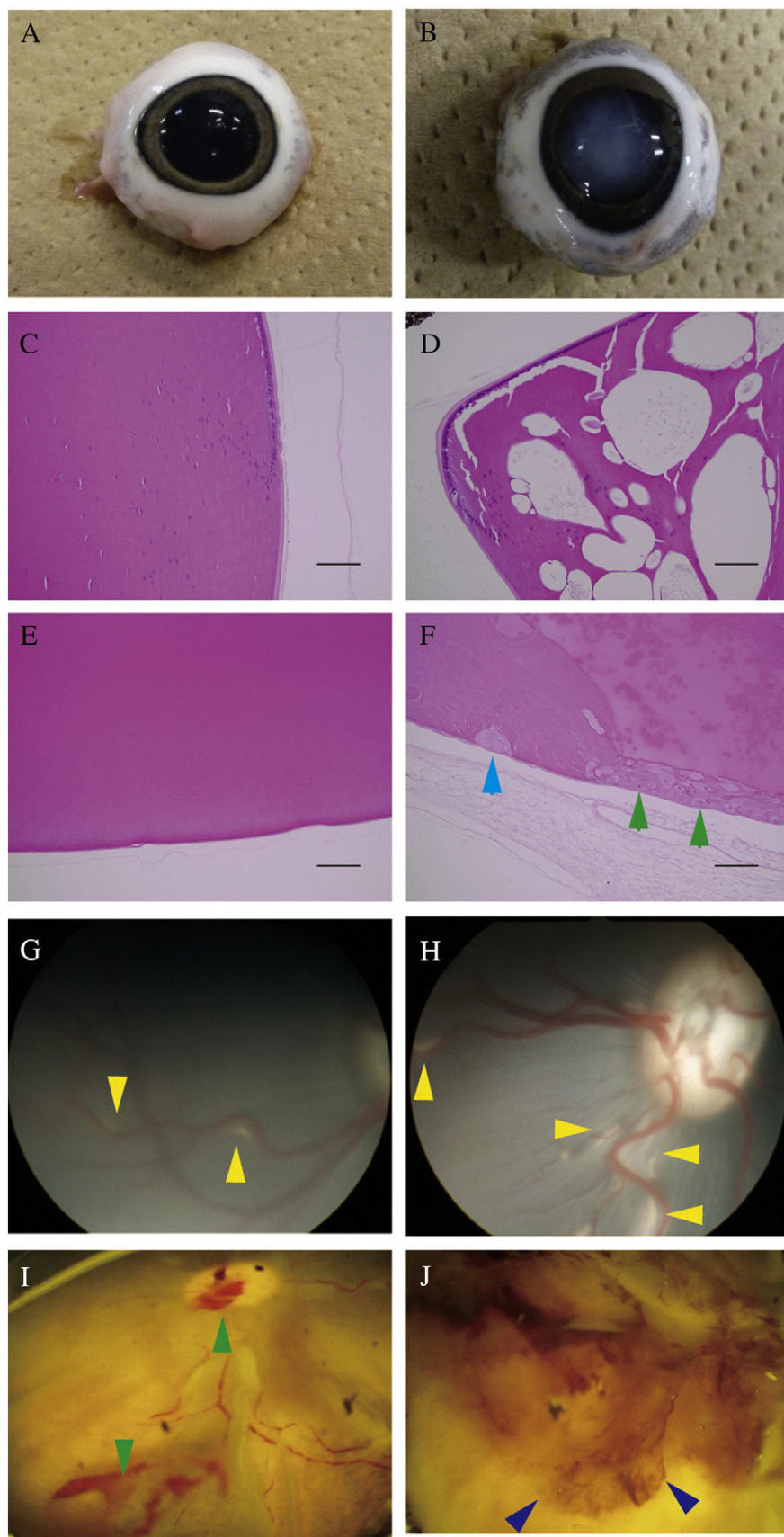


Fig. 2. Ophthalmic pathology of the mutant HNF1 α transgenic pigs. (A and B) The eyes isolated from the WT (A) and DM pigs (B). (C–F) Paraffin-embedded sections of the lens from the WT (C and E) and the DM (D and F) pigs were stained with hematoxylin and eosin. Vacuolization was observed at the equatorial region of the lens (D). Swollen lens fibers and nucleated cells, as indicated with blue and green arrows, respectively, were detected in the lens of the DM pigs (F). (G–J) Ophthalmoscopy of the eye fundus in DM pigs. Cotton-wool spots are indicated with yellow arrows (G and H). Vitreous hemorrhage (I) and neovascular membrane-like lesions (J) are indicated with green and blue arrows, respectively. Scale bar = 100 μ m (C–F). WT, wild type; DM, diabetes mellitus.

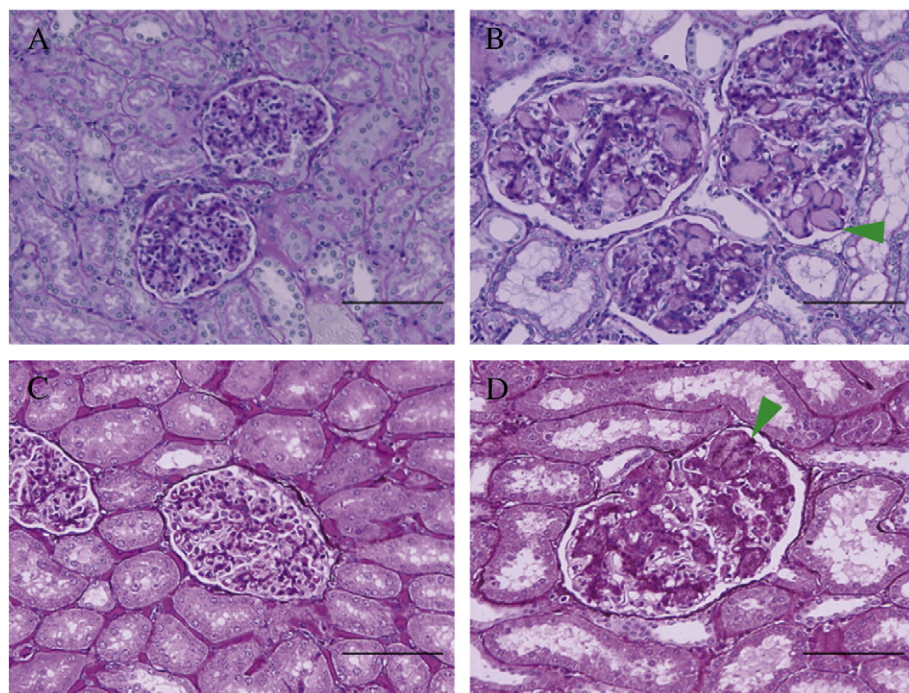


Fig. 3. Histopathological analysis of the kidney of the mutant HNF1 α transgenic pigs. Paraffin-embedded sections were stained with periodic acid-Schiff (A and B) and with periodic acid-methenamine-silver (C and D). Nodular lesions, as indicated with green arrows, were observed in the sections of the DM pigs (B and D), but not in the sections of the WT pigs (A and C). Scale bar = 100 μ m. WT, wild type; DM, diabetes mellitus.

pigs that we developed, lesions very similar to the nodular lesions observed in human diabetic nephropathy were identified at 4.5 months of age.

MODY3 patients with a mutated HNF1 α gene often develop a serious hyperglycemic state, leading to a high incidence of diabetic retinopathy and diabetic nephropathy.²⁴ The DM pigs that we developed are likely to be optimal for studies of therapy for MODY3 patients because the animals show symptoms similar to those of MODY3 patients. Because MODY3 patients do not show the insulin resistance that is seen in patients with DM type 2, insulin administration can control the blood glucose levels of these patients. In our previous study,³² no nodular lesions appeared in the DM pig that was reared for a long period (15 months) with control of their blood glucose levels (Supplemental Fig. 1). Therefore, the DM pigs that we developed are also likely to be a useful model for development of devices for the control of blood glucose levels.

HNF1 α is expressed in the liver, kidneys, small intestines, spleen, and pancreas. It is a transcription factor that functions as either a homodimer or a heterodimer with HNF1 β . Starting from the N-terminal, HNF1 α is composed of a dimerization domain, DNA-binding domain, and transactivation domain.¹⁹ The human HNF1 α dominant-negative mutant P291fsinsC expressed in our DM pigs has normal dimerization and DNA-binding domains but lacks a transactivation domain. The dominant-negative mutant protein derived from the introduced transgene generates an inactive form of the heterodimer by binding to endogenous HNF1 α or HNF1 β thereby inhibits their transcriptional activity.³⁷ It is therefore hypothesized that organs and tissues with higher expression of endogenous HNF1 α or HNF1 β may be affected by the products of the mutant HNF1 α , while tissues lacking endogenous HNF1 α or HNF1 β expression are unaffected.

The likely reason for the growth retardation observed in our pigs that developed DM due to the expression of the mutant HNF1 α gene is the reduced insulin production arising from pancreatic islet cell hypoplasia and insufficient IGF-1 secretion from the liver. HNF1 α influences transcriptional regulation of IGF-1 through the HNF1 α binding consensus sequence on the IGF-1 promoter.^{15,20,22} Insulin and

IGF-1, via their respective receptors, activate the I3K/AKT pathway related to cell growth and survival.²⁸ Indeed, HNF1 α knockout mice were also reported to have low blood IGF-1 levels, similar to our DM pigs.¹⁵

However, the pathological images of the retina and renal glomerulus observed in DM pigs are likely not caused directly by mutant HNF1 α but by complications resulting from diabetes. In the wall of the pig eye, which consists of sclera, choroid, and retina, the expression of normal endogenous HNF1 α and HNF1 β was not detected (Supplemental Fig. 2). Furthermore, normal endogenous HNF1 α and HNF1 β were not expressed in glomerular tissues in the pig kidney.¹⁰ Therefore, although the dominant-negative mutant is ubiquitously expressed in DM pigs, it likely has no direct influence on the wall of the eye and glomerular tissues because there is no target to inhibit.

In conclusion, we established a strain of mutant HNF1 α tg pigs that consistently develop hyperglycemia due to a remarkable attrition of pancreatic β -cells. These DM pigs are characterized by the development of complications similar to those of human DM patients, such as diabetic retinopathy, cataract, and nodular lesions in the renal glomeruli. No other large animal model in which these complications appear relatively early on, has been reported. The DM pigs that we developed will be useful as animal models for studies on the development and progression of DM and the mechanisms underlying the complications of DM and for the evaluating of novel medical technologies, including bionic pancreas and artificial islets.

Acknowledgments

This work was supported by the Meiji University International Institute for Bio-Resource Research and by the Leading Advanced Projects for medical innovation (LEAP), Advanced Research and Development Programs for Medical Innovation (AMED).

Appendix A. Supplementary data

Supplementary data to this article can be found online at <http://dx.doi.org/10.1016/j.jdiacomp.2017.01.025>.

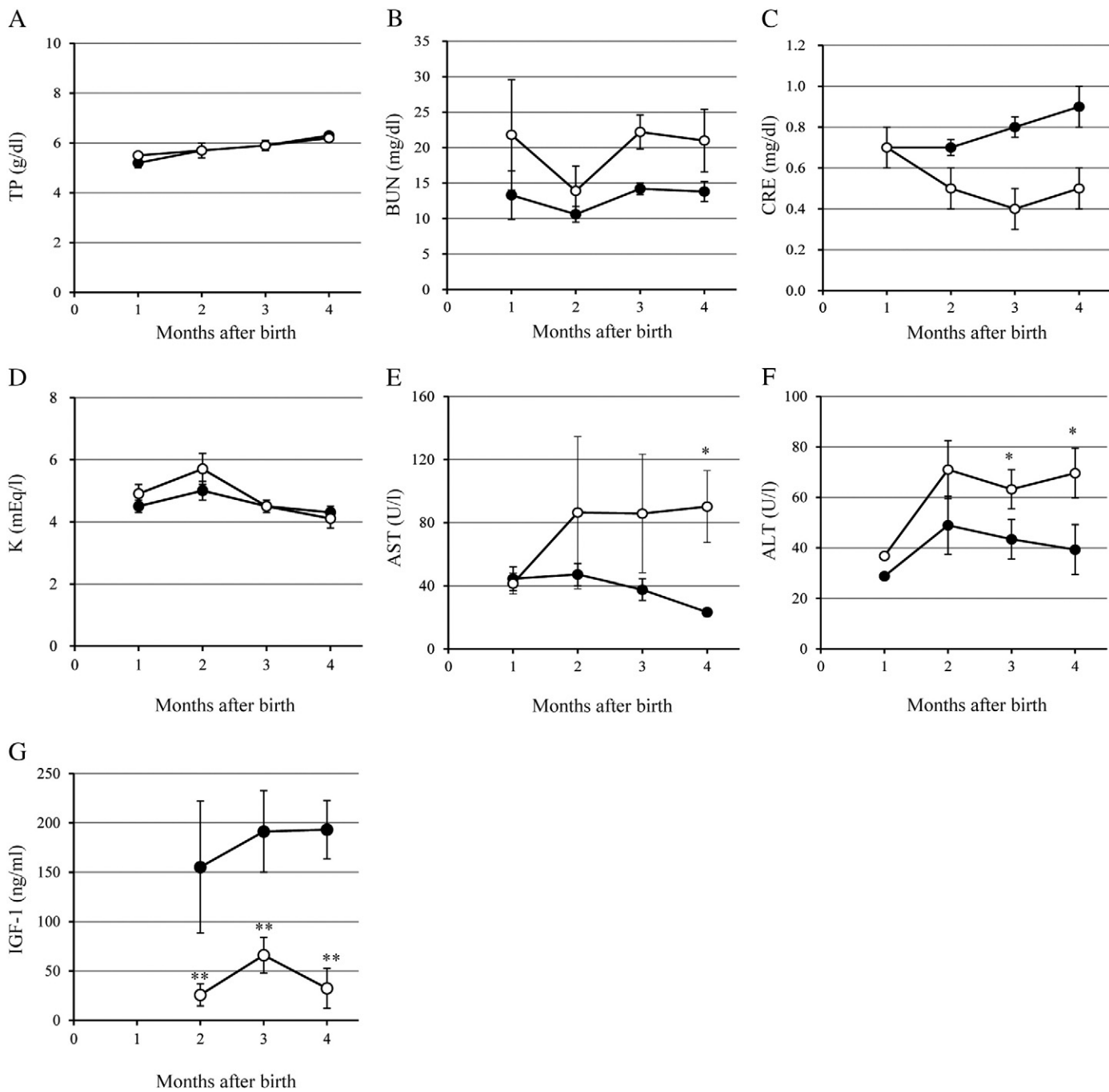


Fig. 4. Biochemical parameters of the WT pigs and the DM pigs. (A) Total protein: TP. (B) Blood urea nitrogen: BUN. (C) Creatinine: CRE. (D) Potassium: K. (E) Aspartate aminotransferase: AST. (F) Alanine aminotransferase: ALT. (G) Insulin-like growth factor 1: IGF-1. Filled and open circles indicate the WT ($n = 5\text{--}8$) and the DM pigs ($n = 4\text{--}5$), respectively. Data shown are presented as the mean \pm SE. * $P < 0.05$, ** $P < 0.01$. WT, wild type; DM, diabetes mellitus.

References

- Bell GI, Polonsky KS. Diabetes mellitus and genetically programmed defects in beta-cell function. *Nature*. 2001;414:788–91.
- Brosius III FC, Alpers CE, Bottinger EP, Breyer MD, Coffman TM, Gurley SB, et al. Mouse models of diabetic nephropathy. *J Am Soc Nephrol*. 2009;20:2503–12.
- Chen YH, Chen HS, Tarng DC. More impact of microalbuminuria on retinopathy than moderately reduced GFR among type 2 diabetic patients. *Diabetes Care*. 2012;35:803–8.
- Cheung N, Mitchell P, Wong TY. Diabetic retinopathy. *Lancet*. 2010;376:124–36.
- Dixon JL, Stoops JD, Parker JL, Laughlin MH, Weisman GA, Sturek M. Dyslipidemia and vascular dysfunction in diabetic pigs fed an atherogenic diet. *Arterioscler Thromb Vasc Biol*. 1999;19:2981–92.
- Fajans SS, Bell GI, Polonsky KS. Molecular mechanisms and clinical pathophysiology of maturity-onset diabetes of the young. *N Engl J Med*. 2001;345:971–80.
- Fioretto P, Mauer M. Histopathology of diabetic nephropathy. *Semin Nephrol*. 2007;27:195–207.
- Furuichi K, Hisada Y, Shimizu M, Okumura T, Kitagawa K, Yoshimoto K, et al. Matrix metalloproteinase-2 (MMP-2) and membrane-type 1 MMP (MT1-MMP) affect the remodeling of glomerulosclerosis in diabetic OLETF rats. *Nephrol Dial Transplant*. 2011;26:3124–31.
- Gerrity RG, Natarajan R, Nadler JL, Kimsey T. Diabetes-induced accelerated atherosclerosis in swine. *Diabetes*. 2001;50:1654–65.
- Hara S, Umeyama K, Yokoo T, Nagashima H, Nagata M. Diffuse glomerular nodular lesions in diabetic pigs carrying a dominant-negative mutant hepatocyte nuclear factor 1-alpha, an inheritant diabetic gene in humans. *PLoS One*. 2014;9:e92219.
- Inagi R, Yamamoto Y, Nangaku M, Usuda N, Okamoto H, Kurokawa K, et al. A severe diabetic nephropathy model with early development of nodule-like lesions induced by megxin overexpression in RAGE/iNOS transgenic mice. *Diabetes*. 2006;55:356–66.
- Jackson PGG, Cockcroft PD. *Handbook of Pig Medicine*. Philadelphia: Elsevier. 2007:259–61.

13. Lai AK, Lo AC. Animal models of diabetic retinopathy: summary and comparison. *J Diabetes Res.* 2013;2013:106594.
14. Larsen MO, Rolin B. Use of the Gottingen minipig as a model of diabetes, with special focus on type 1 diabetes research. *ILAR J.* 2004;45:303–13.
15. Lee YH, Sauer B, Gonzalez FJ. Laron dwarfism and non-insulin-dependent diabetes mellitus in the Hnf-1alpha knockout mouse. *Mol Cell Biol.* 1998;18:3059–68.
16. Lenzen S. The mechanisms of alloxan- and streptozotocin-induced diabetes. *Diabetologia.* 2008;51:216–26.
17. Lunney JK. Advances in swine biomedical model genomics. *Int J Biol Sci.* 2007;3:179–84.
18. Luo Y, Lin L, Bolund L, Jensen TG, Sørensen CB. Genetically modified pigs for biomedical research. *J Inherit Metab Dis.* 2012;35:695–713.
19. Mendel DB, Crabtree GR. HNF-1, a member of a novel class of dimerizing homeodomain proteins. *J Biol Chem.* 1991;266:677–80.
20. Muller M, Brem G. Nucleotide sequence of porcine insulin-like growth factor 1:5' untranslated region, exons 1 and 2 and mRNA. *Nucleic Acids Res.* 1990;18:364.
21. National Agriculture and Bio-oriented Research Organization. *Japanese Feeding Standard for Swine (2005).* Tokyo: Japan Livestock Industry Association. 2005.
22. Nolten IA, Steenbergh PH, Sussenbach JS. Hepatocyte nuclear factor 1 alpha activates promoter 1 of the human insulin-like growth factor I gene via two distinct binding sites. *Mol Endocrinol.* 1995;9:1488–99.
23. Obrosova IG, Chung SS, Kador PF. Diabetic cataracts: mechanisms and management. *Diabetes Metab Res Rev.* 2010;26:172–80.
24. Olek K. Maturity-onset diabetes of the young: an update. *Clin Lab.* 2006;52:593–8.
25. Renner S, Braun-Reichhart C, Blutke A, Herbach N, Emrich D, Streckel E, et al. Permanent neonatal diabetes in INS(C94Y) transgenic pigs. *Diabetes.* 2013;62:1505–11.
26. Renner S, Fehlings C, Herbach N, Hofmann A, von Waldhausen DC, Kessler B, et al. Glucose intolerance and reduced proliferation of pancreatic beta-cells in transgenic pigs with impaired glucose-dependent insulinotropic polypeptide function. *Diabetes.* 2010;59:1228–38.
27. Richter M, Gussetti F, Spiess B. Aldose reductase activity and glucose-related opacities in incubated lenses from dogs and cats. *Am J Vet Res.* 2002;63:1591–7.
28. Siddle K. Signalling by insulin and IGF receptors: supporting acts and new players. *J Mol Endocrinol.* 2011;47:R1–10.
29. Stump KC, Swindle MM, Saudek CD, Strandberg JD. Pancreatectomized swine as a model of diabetes mellitus. *Lab Anim Sci.* 1988;38:439–43.
30. Swindle MM. *Swine in the Laboratory: Surgery, Anesthesia, Imaging, and Experimental Techniques.* 2nd ed. Boca Raton: CRC Press. 2007:141–7.
31. Tian XC, Park J, Bruno R, French R, Jiang L, Prather RS. Altered gene expression in cloned piglets. *Reprod Fertil Dev.* 2009;21:60–6.
32. Umeyama K, Honda K, Matsunari H, Nakano K, Hidaka T, Sekiguchi K, et al. Production of diabetic offspring using cryopreserved epididymal sperm by in vitro fertilization and intrafallopian insemination techniques in transgenic pigs. *J Reprod Dev.* 2013;59:599–603.
33. Umeyama K, Saito H, Kurome M, Matsunari H, Watanabe M, Nakauchi H, et al. Characterization of the ICSI-mediated gene transfer method in the production of transgenic pigs. *Mol Reprod Dev.* 2012;79:218–28.
34. Umeyama K, Watanabe M, Saito H, Kurome M, Tohi S, Matsunari H, et al. Dominant-negative mutant hepatocyte nuclear factor 1alpha induces diabetes in transgenic-cloned pigs. *Transgenic Res.* 2009;18:697–706.
35. Vaca G, Alonso R, Zuniga P, Gonzalez-Quiroga G, Chavez MA, Medina C, et al. Sorbitol dehydrogenase deficiency in several pig tissues: potential implications for studies of experimental diabetes. *Diabetologia.* 1984;27:482–3.
36. Watanabe M, Umeyama K, Kawano HO, Izuno N, Nagashima H, Miki K. The production of a diabetic mouse using constructs encoding porcine insulin promoter-driven mutant human hepatocyte nuclear factor-1alpha. *J Reprod Dev.* 2007;53:189–200.
37. Yamagata K, Yang Q, Yamamoto K, Iwahashi H, Miyagawa J, Okita K, et al. Mutation P291fsinsC in the transcription factor hepatocyte nuclear factor-1 α is dominant negative. *Diabetes.* 1998;47:1231–5.
38. Yang X, Smith SL, Tian XC, Lewin HA, Renard JP, Wakayama T. Nuclear reprogramming of cloned embryos and its implications for therapeutic cloning. *Nat Genet.* 2007;39:295–302.
39. Zhao HJ, Wang S, Cheng H, Zhang MZ, Takahashi T, Fogo AB, et al. Endothelial nitric oxide synthase deficiency produces accelerated nephropathy in diabetic mice. *J Am Soc Nephrol.* 2006;17:2664–9.

SCIENTIFIC REPORTS



OPEN

Generation of heterozygous fibrillin-1 mutant cloned pigs from genome-edited foetal fibroblasts

Received: 29 October 2015

Accepted: 29 March 2016

Published: 14 April 2016

Kazuhiro Umeyama^{1,2}, Kota Watanabe³, Masahito Watanabe^{1,2}, Keisuke Horiuchi^{3,4}, Kazuaki Nakano², Masateru Kitashiro³, Hitomi Matsunari^{1,2}, Tokuhiro Kimura^{5,†}, Yoshimi Arima⁶, Oltea Sampetrean⁶, Masaki Nagaya¹, Masahiro Saito⁷, Hideyuki Saya⁶, Kenjiro Kosaki⁸, Hiroshi Nagashima^{1,2} & Morio Matsumoto³

Marfan syndrome (MFS) is an autosomal dominant genetic disease caused by abnormal formation of the extracellular matrix with an incidence of 1 in 3,000 to 5,000. Patients with Marfan syndrome experience poor quality of life caused by skeletal disorders such as scoliosis, and they are at high risk of sudden death from cardiovascular impairment. Suitable animal models of MFS are essential for conquering this intractable disease. In particular, studies employing pig models will likely provide valuable information that can be extrapolated to humans because of the physiological and anatomical similarities between the two species. Here we describe the generation of heterozygous fibrillin-1 (*FBN1*) mutant cloned pigs (+/Glu433AsnfsX98) using genome editing and somatic cell nuclear transfer technologies. The *FBN1* mutant pigs exhibited phenotypes resembling those of humans with MFS, such as scoliosis, pectus excavatum, delayed mineralization of the epiphysis and disrupted structure of elastic fibres of the aortic medial tissue. These findings indicate the value of *FBN1* mutant pigs as a model for understanding the pathogenesis of MFS and for developing treatments.

FBN1 encodes fibrillin-1 (FBN1), which is a 350-kDa glycoprotein comprising 2,871 amino acid residues. FBN1 is the principal structural component of extracellular microfibrils^{1–3} and is distributed throughout the body as a connective-tissue matrix of tissues such as skin, lung, kidney, vessels, cartilage, tendon, muscle, cornea, and ciliary zonule¹. FBN1 is intimately involved in the transforming growth factor-β (TGF-β) signalling pathway, which is essential for cell proliferation and differentiation. TGF-β1 binds to fibrillin-1 via the latent TGF-β-binding protein (LTBP) and controls signalling through this pathway by inhibiting the binding of TGF-β1 to its receptor^{4,5}.

Marfan syndrome (MFS) (OMIM #154700) is an autosomal-dominant disorder of connective tissue caused by mutations of *FBN1*^{6,7}. The symptoms of MFS manifest principally as cardiovascular and skeletal abnormalities. The primary cause of death of patients with MFS is progressive aortic dilation, principally in the sinus of Valsalva, leading to aortic dissection or rupture^{8,9}. Skeletal symptoms include a tall and thin physique, long limbs, arachnodactyl, thoracic deformity (pectus carinatum, pectus excavatum), scoliosis, a high-arched palate, and chronic joint laxity. Other symptoms include ectopia lentis and myopia, skin striae atrophicae, and recurrent hernia or pneumothorax^{8,9}.

Studies of *FBN1* mutant mice^{10–14} have contributed valuable information regarding the causes of MFS and for the development of treatments. However, small animals such as rodents are inadequate as models for humans to guide development of treatments involving surgical techniques to address cardiovascular or skeletal system

¹Meiji University International Institute for Bio-Resource Research, Kawasaki, 214–8571, Japan. ²Laboratory of Developmental Engineering, Department of Life Sciences, School of Agriculture, Meiji University, Kawasaki, 214–8571, Japan. ³Department of Orthopaedic Surgery, Keio University School of Medicine, Tokyo, 160–8582, Japan.

⁴Anti-aging Orthopaedic Research, Keio University School of Medicine, Tokyo, 160–8582, Japan. ⁵Department of Pathology, Keio University School of Medicine, Tokyo, 160–8582, Japan. ⁶Division of Gene Regulation, Institute for Advanced Medical Research, Keio University School of Medicine, Tokyo, 160–8582, Japan. ⁷Division of Operative Dentistry, Department of Restorative Dentistry, Tohoku University Graduate School of Dentistry, Sendai, 980–8575, Japan. ⁸Center for Medical Genetics, Keio University School of Medicine, Tokyo, 160–8582, Japan. [†]Present address: Department of Pathology, Yamaguchi University Graduate School of Medicine, Ube-shi, 755–8505, Japan.

Correspondence and requests for materials should be addressed to H.N. (email: hnagas@meiji.ac.jp) or M.M. (email: morio@a5.keio.jp)

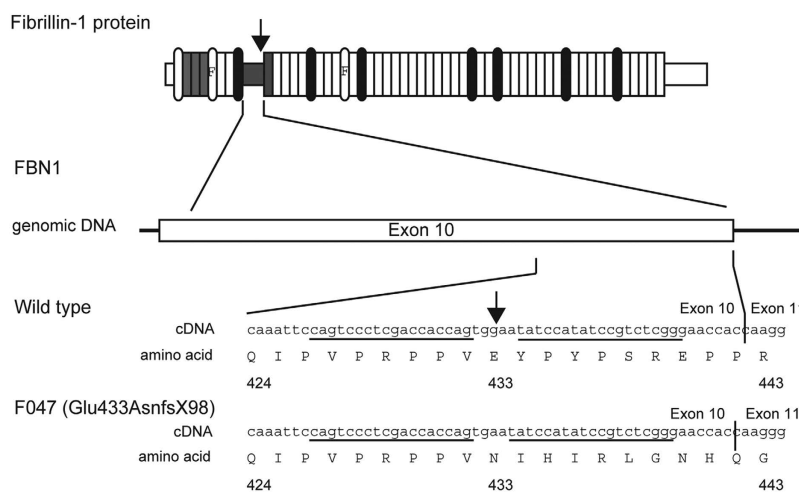


Figure 1. Schematic representation of porcine *FBN1* showing the cleavage site for the zinc finger nuclease FBN1ZFN05. Arrows indicate the cleavage sites for the ZFN. The ZFN recognition sequence is underlined.

manifestations. Therefore, large animals exhibiting a phenotype similar to the cardiovascular and skeletal manifestations of patients with MFS may contribute to the development of new treatments of patients with MFS and for gaining further insights into the pathogenesis of this intractable disease.

The application of recently developed genome editing and somatic cell cloning techniques has markedly improved the efficiency of generating pigs with gene mutations^{15–24}. In the present study, we generated heterozygous *FBN1* mutant cloned pigs and their progeny, and showed that they developed phenotypes resembling those of patients with MFS.

Results

Generation of heterozygous *FBN1* mutant cell lines. We used electroporation to introduce an mRNA encoding the zinc finger nuclease (ZFN) FBN1ZFN05 that targets exon 10 of *FBN1*, which encodes a proline-rich region C (Fig. 1). Seven and 13 clones of homozygous and heterozygous mutants, respectively, which were isolated from 480 colonies, did not display detectable changes in cell shape or proliferation compared with the parental cells (Table 1). We selected the heterozygous *FBN1* mutant clone F047 (+/Glu433AsnfsX98), which encodes a putative truncated *FBN1* caused by a 1-bp deletion of a guanine nucleotide that creates a stop codon at amino acid residue 531 (Fig. 1, Fig. S1), to serve as the nuclear donor.

Generation of cloned piglets with a heterozygous mutant of *FBN1*. *FBN1* mutant cloned piglets with syngeneic backgrounds were created from embryos reconstructed via somatic cell nuclear transfer (SCNT) of heterozygous *FBN1* mutant cells (F047).

In the first experiment, we confirmed that 62.0% (245/395) of the SCNT embryos could develop to the blastocyst stage after *in vitro* culture for 5–6 days. The cloned blastocysts obtained were transferred into two recipients (103 embryos/recipient), and both recipients carried their pregnancies through birth, bearing seven live and one dead offspring (Table 2).

In the second experiment, 334 of the SCNT embryos were cultured *in vitro* for 1–2 days, and 272 embryos at the 1- to 2-cell stage were then transferred into two recipient gilts (136 embryos/recipient). Both recipients became pregnant, and they farrowed a total of 10 live and one stillborn piglets (Table 2).

In both experiments, the efficiencies of generating *FBN1* mutant cloned piglets from SCNT embryos (8/206, 3.9% and 11/272, 4.0%) were within the range of those normally achieved by our laboratory (1.4–4.3%)^{25–27}. All *FBN1* mutant cloned piglets harboured the same *FBN1* mutation and were the same sex as the F047 nuclear donor cells (Fig. S1). However, the phenotypes of the *FBN1* mutant cloned pigs obtained in the two experiments differed strikingly as described below.

Phenotypes of heterozygous *FBN1* mutant cloned pigs derived from blastocysts. Phenotypic abnormalities in the *FBN1* mutant cloned pigs obtained after transfer of the cloned blastocysts are presented in Table 3. Of the 8 neonatal piglets (including 1 stillborn), 3 exhibited external abnormalities including pectus excavatum (Fig. 2E) or cleft palate (Fig. S2). One of these animals showed both abnormalities.

Four piglets were analysed for skeletal abnormalities by computed tomography (CT) within 3 days after birth. Delayed mineralization in the epiphysis of the os coxa, femur, tibia, fibula, and humerus (Fig. 2G,H) was observed in one animal. Furthermore, the thoraxes of the mutant piglets were nearly conical, whereas the thoraxes of the WT piglets were barrel-shaped. No abnormalities of the spine were observed (Fig. 2B,F).

Aortic abnormalities were also detected in some of the *FBN1* mutant animals following Elastica van Gieson (EVG) staining of the wall tissue of the proximal thoracic aorta (Fig. 3). The aortic media of the control WT pigs contained a large number of wavy elastic fibres arranged vertically in an orderly structure (Fig. 3A,B). Extensive collagenous connective tissue that stained red was detected between these elastic fibres (Fig. 3A,B). In contrast,

Wild type genomic DNA		
	CAGTCCCTCGACCACCACTGGAAATATCCATATCCGTCTCGG	
FBN1 ZFN05 binding sequence		
	CAGTCCCTCGACCACCA <u>Gnnnnn</u> TATCCATATCCGTCTCGG	
Homozygous mutants		
F038	CAGTCCCTCGACCACCA <u>G</u> ****TATCCATATCCGTCTCGG	5bp del
F063	CAGTCCCTCGACCA***** <u>T</u> CCATATCCGTCTCGG	11bp del
F162	CAGTCCCTCGACCA***** <u>T</u> ATCCGTCTCGG	15bp del
F007	CAGTCCCTCGACC <u>A</u> GGATATCCATATCCGTCTCGG	4bp sub
	CAGTCCCTCGACCAC***** <u>A</u> TATCCGTCTCGG	13bp del
F022	CAGTCCCTCGACCACCA <u>G</u> ***ATATCCATATCCGTCTCGG	4bp del
	CAGTCCCTCGACC***** <u>T</u> GGAA <u>T</u> ATCCATATCCGTCTCGG	5bp del
F083	CAGTCCCTCGACCAC***** <u>G</u> GAATATCCATATCCGTCTCGG	4bp del
	CAGTCCCTCGACCAC***** <u>C</u> ATATCCGTCTCGG	14bp del
F117	CAGTCCCTCGACCACCA***** <u>T</u> ATCCGTCTCGG	12bp del
	CAGTCCCTCGACCACCA***** <u>T</u> CCGTCTCGG	13bp del
Heterozygous mutants		
F002	CAGTCCCTCGACCACCA***(111bp del)**TTAAGTCA	111bp del
F005	CAGTCCCTCGACCACCA <u>G</u> GTGG <u>A</u> ATATCCATATCCGTCTCGG	4bp ins
F013	CAGTCCCTCGACCACCA <u>G</u> **AATATCCATATCCGTCTCGG	3bp del
F020	CAGTCCCTCGACCACCA <u>G</u> ****ATCCATATCCGTCTCGG	5bp del
F029	CAGTCCCTCGACCA***(63del + 7bp ins)**CTTTTC	56bp del
F035	CAGTCCCTCGACCACCA <u>G</u> GTG***TATCCATATCCGTCTCGG	3bp del
F036	CAGTCCCTCGACCACCA <u>G</u> GTGA <u>A</u> ATATCCATATCCGTCTCGG	5bp ins
F041	CAGTCCCTCGACCACCA <u>G</u> ***ATATCCATATCCGTCTCGG	4bp del
F043	CAGTCCCTCGACCACCA*****TATCCATATCCGTCTCGG	6bp del
F047	CAGTCCCTCGACCACCA <u>G</u> GTG*AA <u>T</u> ATCCATATCCGTCTCGG	1bp del
F050	CAGTCCCTCGACCACCA <u>G</u> AA <u>T</u> ATCCATATCCGTCTCGG	2bp del
F074	CAGTCCCTCGACCACCA <u>G</u> AA <u>T</u> CCATATCCGTCTCGG	1bp del
F098	CAGTCCCTCGACCACCA <u>G</u> ***ATATCCATATCCGTCTCGG	4bp del

Table 1. Sequencing assay for ZFN-induced mutations in the FBN1-targeted region. Multiple deletions or insertions depicted using asterisks or underlines, respectively.

<i>In vitro</i> development of SCNT embryos				
SCNT embryos reconstructed		395	334	
Early cleavage-stage embryos		302	272 ^b	
Blastocyst-stage embryos on day 5		245 ^a	–	
Production of heterozygous <i>FBN1</i> mutant cloned piglets				
Recipient	#R1 ^a	#R2 ^a	#R3 ^b	#R4 ^b
Embryos transferred	103	103	136	136
Pregnancy	+	+	+	+
No. of viable cloned piglet	4	3	2	8
No. of stillborn cloned piglet	0	1	1	0

Table 2. *In vitro* development of SCNT embryos and production of heterozygous *FBN1* mutant cloned piglets. ^aThe SCNT embryos cultured for 5 to 6 days were transferred to the recipients' uteri. ^bThe SCNT embryos cultured for 1 to 2 days were transferred to the recipients' oviducts.

the elastic fibres of the aortic medial tissues of the *FBN1* mutant piglets (Fig. 3E,F) exhibited fragmented, discontinuous structures. Furthermore, there was only a sparse collagenous connective tissue layer within the elastic fibre structure (Fig. 3E,F). Immunohistochemical analyses using anti-FBN1 and anti-FBN2 antibodies revealed that the intensity of FBN1-positive microfibrils was lower in the aortic wall medial tissue of the *FBN1* mutant cloned piglets (Fig. 3G) compared with those from the WT piglets (Fig. 3C). In contrast, FBN2 was detected in the tissues of the *FBN1* mutant cloned piglets (Fig. 3H), although it was undetectable in those of the WT controls (Fig. 3D). These histological abnormalities were not detected in the distal thoracic aorta.

Dilation of the sinus of Valsalva and proximal thoracic aorta, as observed in patients with MFS, was not observed in these pigs. No individuals were found to have developed the ectopia lentis generally observed in patients with MFS. Two of the 7 live cloned offspring grew normally beyond sexual maturity.

Piglet No.	Birth weight (kg)	Postpartum survival (day)	Neonatal phenotypic abnormalities	Phenotypic features
Embryo transfer at 5 or 6 days				
#1	1.088	551 ^e	—	Quadriplegia
#2	1.051	19 ^u	+	Fragmentation of elastic fibers*, Pectus excavatum*
#3	0.550	68 ^u	—	
#4	0.536	1 ^e	+	Cleft palate, Fragmentation of elastic fibers*, Pectus excavatum*
#5	0.858	738 ^e	—	
#6	0.911	3 ^u	+	Delayed bone mineralization*
#7	0.944	0 ^s	+	Cleft palate
#8	0.811	0 ^u	—	
Embryo transfer at 1 or 2 days				
#9	1.481	90 ^e	—	Quadriplegia
#10	1.247	520 ^e	—	Pectus excavatum*, Quadriplegia
#11	0.506	0 ^s	—	
#12	0.855	4 ^u	—	
#13	0.956	76 ^e	—	Distressed breathing, Quadriplegia
#14	0.605	0 ^u	—	
#15	0.875	412 ^e	—	Scoliosis*
#16	1.210	3 ^u	—	
#17	1.158	0 ^e	—	
#18	0.781	38 ^u	—	
#19	0.849	66 ^e	—	Nystagmus, Quadriplegia

Table 3. Phenotypes of heterozygous *FBN1* mutant cloned piglets. ^eEuthanatized. ^sStillborn. ^uThe cause of death is unknown. *Marfan-like symptoms.

Phenotypes of heterozygous *FBN1* mutant cloned pigs derived from early-cleavage stage embryos. No external abnormalities were apparent in any of the 11 *FBN1* mutant neonates (including 1 stillborn) obtained after transfer of the cloned embryos at the early cleavage stages (Table 3). CT analysis of 5 piglets within 4 days after birth detected no skeletal abnormalities.

Three of the cloned pigs exhibited symptoms of gait disturbance, nystagmus, distressed breathing, and quadriplegia and were therefore euthanized at ages ranging from 66 to 90 days. The cause of these abnormalities was unknown.

Two pigs grew to beyond sexual maturity. One was found to exhibit a spinal deformity (Fig. 4B) and abnormal gait at 145 days of age. This pig exhibited astasia at 399 days of age and was therefore euthanized. Scoliosis of the spine was recognized at autopsy, and a CT scan of the spinal column revealed that the normal vector of the plane formed by the superior margin and that of the plane formed by the inferior margin of the lumbar vertebra (second lumber: L2) were offset by 6.5° (normal alignment in pigs, 1.5°) as shown in Fig. 4C,D. The other pig was euthanized at 520 days of age when it exhibited astasia. Pectus excavatum was found at autopsy, although it was not apparent at the neonatal stage.

Generation of heterozygous and homozygous *FBN1* mutant progeny. We mated heterozygous *FBN1* mutant cloned pigs (founder males) and WT females to produce male and female heterozygous *FBN1* mutant offspring in the first-generation (G1) progeny (Fig. S3). Additionally, the G2 progeny were generated by mating the G1 animals (Fig. S1D, S3, S7A). The G2 offspring comprised homozygous *FBN1* mutants, heterozygous *FBN1* mutants, and wild-type individuals, per Mendelian inheritance principles. The incidence (3 of 12, Table S1) of the heterozygous *FBN1* mutant pigs exhibiting the MFS-like symptoms in the G1 and G2 progeny was similar to that in the founder cloned pigs generated from the short-cultured SCNT embryos (2 of 11). The G2 homozygous mutant pigs showed typical symptoms of MFS, such as dilatation of the ascending aorta and rupture of the elastic lamina (Fig. S4), aortic dissection (Fig. S5), ectopia lentis (Fig. S6), and lipodystrophy (Fig. S7). Similar to the MFS mouse model^{10–12}, the homozygous mutation conferred neonatal lethality (longest survival time: 28 days). Furthermore, by examining the levels of *FBN1* mRNA expressed in fibroblasts isolated from these animals, we confirmed that the mRNA had been degraded, probably through a nonsense-mediated mRNA decay (NMD) mechanism (Fig. S8).

Discussion

There are more than 3,000 documented mutations of human *FBN1* (<http://www.umd.be/FBN1/>). Patients with MFS with a heterozygous *FBN1* mutation that generates a truncated form of FBN1 (Arg429X, Tyr434X) exhibit typical MFS pathology of the skeleton, eyes, and blood vessels as well as symptoms of scoliosis and dilation of the arteries^{28,29}. In the present study, to develop an animal model to better understand the pathogenesis of MFS, we generated cloned pigs heterozygous for a mutant *FBN1* (Glu433AsnfsX98).

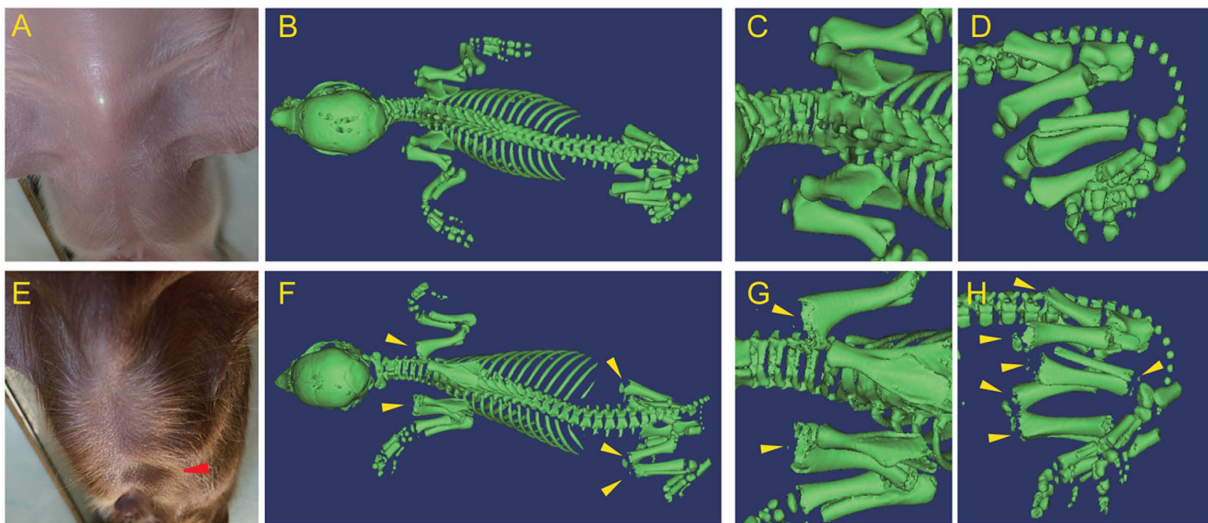


Figure 2. Skeletal abnormalities of the heterozygous *FBN1* mutant cloned pigs. (A,E) Appearance of the thorax of a WT pig (A) and an *FBN1* mutant pig with pectus excavatum (E, red arrowhead). (B–D,F–H) Multidetector CT imaging of the skeletal structures of a WT piglet (B–D) and an *FBN1* mutant piglet (#6, F–H). The WT and *FBN1* mutant piglets had a barrel-shaped (B) and a conically shaped (G) thorax, respectively. Delayed mineralization of the primary spongiosa and epiphyseal nucleus (arrowhead) was recognized in the humerus (G), the os coxa (H), the femur (H), and the fibula (H) of the *FBN1* mutant piglet.

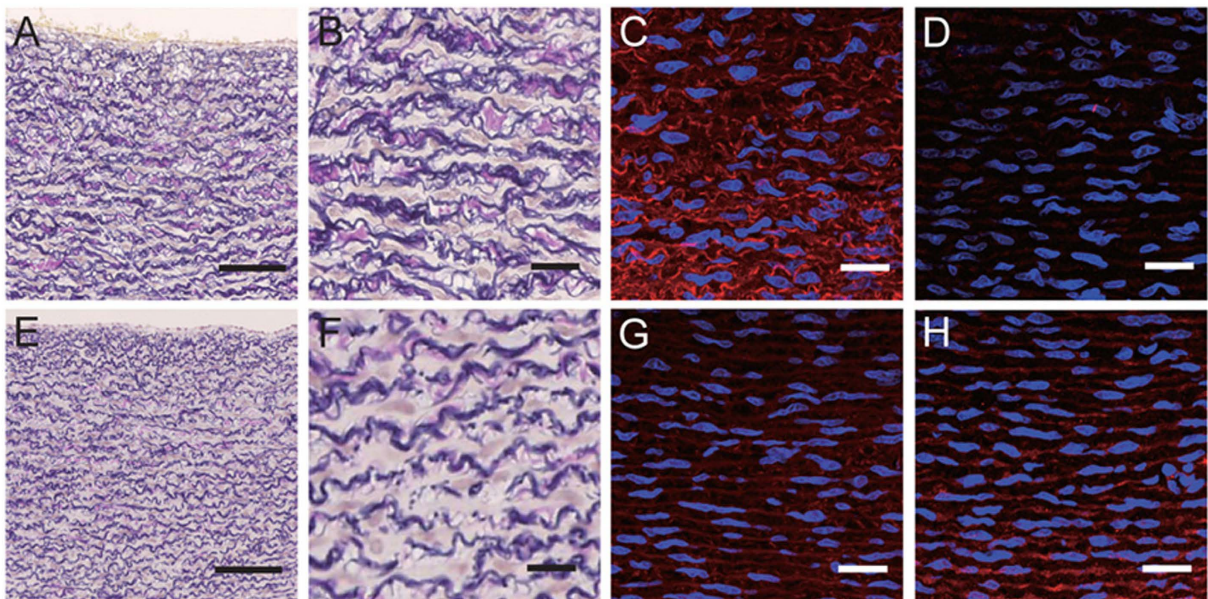


Figure 3. Histology of the proximal thoracic aortic wall of the heterozygous *FBN1* mutant cloned piglets. Proximal thoracic aortic wall of WT (A–D) and heterozygous *FBN1* mutant cloned piglets (E–H). EVG-stained sections from the *FBN1* mutant cloned piglets (E,F) show that the elastic fibres had a fractured and discontinuous structures compared with those of wild-type (WT) piglets (A,B). (C,G) The intensity of staining of FBN1-positive microfibrils was reduced in the aortic wall medial tissue of the mutant piglets (G) compared with that of WT piglets (C). (D,H) FBN2 was undetectable in the aortic wall medial tissue of the WT piglets (D), whereas it was clearly detected in the same tissue of *FBN1* mutant piglets (H). Nuclear staining (DAPI) is shown in blue (C,D,G,H). Scale bars: 100 µm (A,E) and 20 µm (B–D,F–H).

In the present study, heterozygous *FBN1* mutant cloned pigs were generated from a single line of nuclear donor cells; therefore, all cloned animals were siblings with the same genetic background and the same mutation. However, the cloned piglets did not exhibit a homogenous phenotype. The relationship between MFS genotype and the phenotype is extremely complex, and there are differences in pathology between patients of the same family lineage³⁰. Moreover, heterozygous *FBN1* knockout (KO) mice carrying the same mutation exhibit

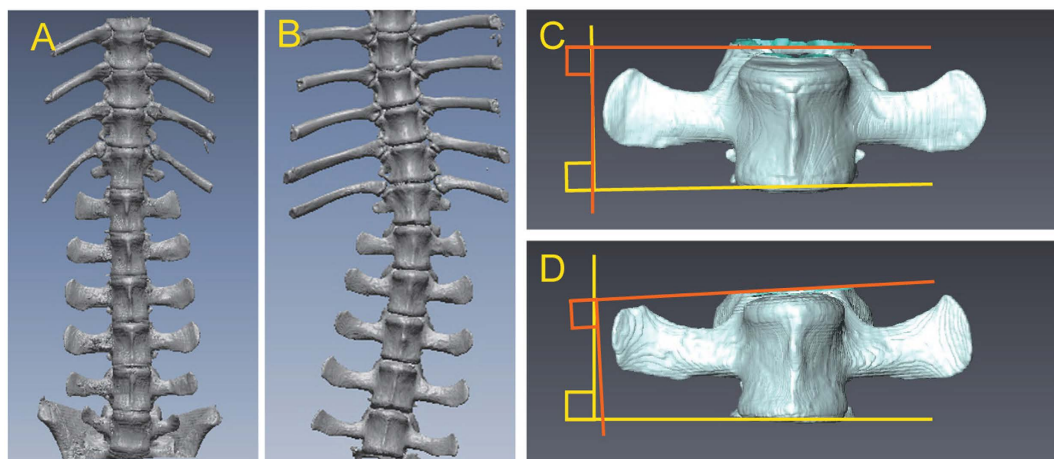


Figure 4. Scoliosis of a *FBN1* mutant cloned pig. **(A,B)** CT image of an *FBN1* mutant cloned pig (#15, **B**) showing scoliosis of the spine, compared with a WT pig (**A**). **(C,D)** CT images of the lumbar vertebrae (L2) of an *FBN1* mutant cloned pig with scoliosis (**D**) indicated that the normal vector of the plane formed by the superior margin of the vertebra and that of the plane formed by the inferior margin were offset by 6.5°. Normal alignment in a WT pig (**C**) was 1.5°.

lineage-specific phenotypic differences, and the severity of disease correlates negatively with the level of *FBN1* mRNA expression. These findings suggest the contribution of both epigenetic and genetic factors to the expression of MFS phenotypes and the severity of symptoms¹³.

Immediately following fertilization, paternal genomic DNA undergoes rapid and progressive demethylation, whereas the maternal genomic DNA undergoes gradual demethylation after postfertilization S-phases^{31,32}. Demethylation progresses until the late morula stage (day 4) followed by remethylation of genomic DNA^{31,32}. Evidence indicates that the characteristic genomic demethylation–methylation pattern that occurs during early development is affected by *in vitro* culture of embryos. For example, pig embryos cultured *in vitro* and embryos that develop *in utero* differ in their expression of 588 genes³³. In the present study, we generated cloned pigs from embryos cultured for 1–2 or 5–6 days. Cloned animals derived from the latter cultures more frequently exhibited MFS-like phenotypes. Epigenetic regulatory patterns of transcription are determined early during embryogenesis³¹. Together, these findings suggest that epigenetic factors might have influenced the phenotypes of the *FBN1* mutant cloned pigs generated here. Therefore, we suggest that these differences in phenotypes can be attributed to lower levels of *FBN1* mRNA synthesized by the single WT allele and that efficient generation of porcine models of MFS may require regulation of epigenetic modifiers in addition to mutation of the causal gene. The transcriptional activity of the WT allele in heterozygous *FBN1* mutant pigs needs to be analysed.

To correctly assess the effects of heterozygous *FBN1* mutation in pigs, founder cloned pigs were crossbred with WT pigs to obtain progeny animals, followed by analysis of the offspring's phenotypes. Because methylation of genomic DNA is normalized by sexual reproduction, this crossbreeding must have eliminated the unnatural epigenetic regulation that resulted from SCNT^{31,32}. Analysis of the progeny animals therefore enabled us to confirm the influence of the mutant gene in isolation. The heterozygous *FBN1* mutation transmitted from the founder cloned pigs to their progeny caused the similar pathological phenotypes, thereby indicating the significance of this mutation in the pig.

In contrast, dominant incidence of the abnormal phenotype in the founder cloned animals generated from the long-cultured SCNT embryos compared to the progeny animals and the clones derived from the short-cultured embryos further indicated the epigenetic influence on the outcome of the heterozygous *FBN1* mutation.

Scoliosis is a major symptom of MFS and affects more than 60% of patients, and 25–50% of these patients suffer from severe deformities that require surgery³⁴. However, the incidence of scoliosis in *FBN1* mutant pigs studied here was lower than that in patients with MFS, and the spinal deformation was less severe. For example, studies of animal models of idiopathic scoliosis indicate that the lower incidence of scoliosis in quadruped animals results from the different directional gravitational force on the spine³⁵ between bipedal humans and quadrupedal pigs. Therefore, this difference likely resulted in the lower incidence and reduced severity of scoliosis in the *FBN1* mutant pigs.

Delayed mineralization of the epiphysis occurred in the *FBN1* mutant pigs studied here, which is consistent with studies of mice showing that *FBN1* expression levels influence bone density. For example, bone volume is reduced in *Fbn1*^{MgR/MgR} mice, which express only 15% of the normal level of *FBN1* because of TGF-β-induced osteoclastogenesis³⁶. Furthermore, bone mineral density and volume are lower in *FBN1*-KO mice than in normal mice¹⁴, and patients with MFS display reduced mineral density of the epiphysis; however, whether or not this contributes to pathogenesis is unknown³⁷. Therefore, a detailed analysis of the bone formation abnormalities that occur in *FBN1* mutant pigs will likely help explain the symptomatology of patients with MFS.

Histopathology of the thoracic aorta is an important characteristic of MFS. For example, dilation of the aorta occurs in 78% of patients with MFS³⁸, and enlargement of the aorta and formation of aneurisms may lead to aortic

rupture. In patients with MFS with aortic aneurisms, fragmentation of the elastic fibres was evident³⁹. Here we observed fragmentation of elastic fibres in the *FBN1* mutant pigs.

Elastic fibres are composed of an elastin core surrounded by microfibrils⁴⁰. FBN2 is present near the centre of the microfibrils, surrounded by FBN1^{41,42}. Consequently, when centrally located FBN2 epitopes appear exterior to the microfibrils, reaction with anti-FBN2 antibodies is induced. We show here using immunohistochemistry that the tunica media of the thoracic aorta of heterozygous *FBN1* mutant cloned pigs expressed low levels of FBN1 but high levels of FBN2. These findings may be explained as follows: (1) the amount of FBN1 decreased because the *FBN1* mRNA had been degraded, and (2) FBN2 molecules near the central parts of the microfibrils were not covered by a sufficient amount of normal FBN1.

In the present study, we generated pigs that were heterozygous for a mutant *FBN1* and exhibited phenotypes resembling the symptoms of human MFS. Furthermore, two groups of cloned siblings with mutated *FBN1* on a syngeneic background showed striking differences in their individual phenotypes, which is consistent with the distinct phenotypes of familial cases of patients with MFS. The manner in which the expression of FBN1 from the remaining allele is regulated is likely critical for establishing the heterozygous *FBN1* mutant pig as a model for human MFS. Consequently, the heterozygous *FBN1* mutant pigs that we generated in the present study will likely prove useful for investigation of the epigenetic modifiers of MFS onset.

Material and Methods

Animal care. The Institutional Animal Care and Use Committee of Meiji University approved the animal experiments described in this study (IACUC12-0008). All animal care and experimental procedures were performed in accordance with Japan Act on Welfare and Management of Animals and regulations. Six crossbred (Large White/Landrace × Duroc) prepubertal gilts served as surrogate mothers for the embryo transfer experiments or as breeder pigs for progeny production. Three male crossbred new-born piglets were used as controls for the *FBN1* mutant cloned piglets. Pigs were housed in a temperature-controlled room, had free access to water and were provided with growth-stage appropriate commercial feed (Chubushiryo Co., Ltd. Nagoya, Japan) in accordance with the Japanese Feeding Standard for Swine (2005)⁴³. The health of all pigs was assessed at feeding (08:00 and 17:00). For autopsies, piglets were anaesthetized using intramuscular injection of ketamine (11 mg/kg, Fujita Pharmaceutical Co., Ltd., Tokyo, Japan). Anaesthesia was maintained via inhalation of isoflurane (DS Pharma animal Health Co., Ltd., Osaka, Japan), and the piglets were exsanguinated. Adult pigs were administered intramuscular injection of 1% mafoprazine mesylate (0.5 mg/kg, DS Pharma animal Health Co., Ltd.) followed by intravenous pentobarbital (Kyoritsu Seiyaku Co., Ltd., Tokyo, Japan), and anaesthesia was maintained via inhalation of isoflurane while the pigs were exsanguinated.

Chemicals. All chemicals were purchased from the Sigma-Aldrich Chemical Co. (St. Louis, MO, USA) unless otherwise indicated.

Design of ZFNs. A custom ZFN mRNA for porcine *FBN1* was obtained from Sigma-Aldrich Chemical Co. The supplier designed and validated the ZFN mRNAs. Each ZFN contained six zinc finger domains recognizing 18 bases (Fig. 1). These sequences displayed high specificity, such that if fewer than 9 of the 36 bases were mismatched, off-target sequences were not recognized. This specificity was confirmed using the porcine genome DNA database Sscrofa9 Ensembl (http://feb2012.archive.ensembl.org/Sus_scrofa/Info/Index) (Table S2).

Isolation of *FBN1* mutant cells and culture conditions. A primary culture of porcine foetal fibroblasts (male, Large White/Landrace × Duroc) was used to isolate *FBN1* mutant cells. The fibroblasts and their derivatives (mutant cells) were seeded on type I collagen-coated dishes or plates (Asahi Glass, Tokyo, Japan) and were cultured in MEM α (Life Technologies, Carlsbad, CA, USA) supplemented with 15% foetal bovine serum (FBS, Nichirei Bioscience, Tokyo, Japan) and 1× antibiotic-antimycotic solution (Life Technologies) in a humidified atmosphere containing 5% CO₂ at 37 °C. The foetal fibroblasts were cultured to 70–90% confluence, washed twice with D-PBS(−) (Life Technologies) and treated with 0.05% trypsin-EDTA (Life Technologies) to isolate and collect the cells. The cells (4 × 10⁵) were then suspended in 40 μL of R buffer (a component of the Neon Transfection System, Life Technologies), and 2 μL of ZFN-encoding mRNA solution (400 ng/μL in RNase-free water) was added. The cells were electroporated as follows: pulse voltage, 1,100 V; pulse width, 30 ms; and pulse number, 1. Following electroporation, the cells were cultured at 32 °C for 3 days (transient cold shock), initially without antibiotics in the medium described above and then with antibiotics after 24 h⁴⁴. For recovery from the transient cold shock, the cells were cultured at 37 °C until they approached confluence. Five 96-well plates were used to prepare a limiting dilution of a cell suspension, and 12 days later, cells that were >50% confluent in each well were selected and subcultured.

Analysis of ZFN-induced mutations in nuclear donor cells and cloned piglets. The target region of *FBN1*-ZFNs was amplified via direct PCR from the cell clones using MightyAmp DNA polymerase (Takara Bio, Shiga, Japan) and the corresponding primers 5'-GACATAGGTGAAGACTTCGTAGG and 5'-TCACTCTCAAGACTCCAGTTGG. Nested PCR was performed using PrimeSTAR HS DNA polymerase (Takara Bio) and the appropriate primers 5'-AACTGAGAGTGACTTCCATGGAC and 5'-GCAACCCTCATTTCTCTATG. The nested PCR fragment from each clone was analysed using the sequencing primer 5'-TAACTTGCTCCAGCTCAGGTG, the BigDye Terminator Cycle Sequencing Kit and an ABI PRISM 3130xl Genetic Analyzer (Life Technologies). The nested PCR fragments that contained the mutation were subcloned into the sequencing vector pCR4Blunt-TOPO (Life Technologies).

For analysis of the mutation in each piglet, genomic DNA was extracted from tail biopsies of the piglets using a DNeasy Tissue and Blood Kit (QIAGEN, Hilden, Germany), and PCR genotyping and DNA sequencing were performed as described above.

Somatic cell nuclear transfer and embryo transfer. SCNT was performed as described previously with slight modifications²⁶. Briefly, *in vitro*-matured oocytes were enucleated via gentle aspiration of the polar body and the adjacent cytoplasm using a bevelled pipette in Tyrode lactose medium containing 10 mM HEPES and 0.3% (w/v) polyvinylpyrrolidone in the presence of 0.1 µg/mL demecolcine, 5 µg/mL cytochalasin B (CB) and 10% FBS.

Nuclear donor cells (clone F047) were used following cell-cycle synchronization induced by serum starvation for two days. A single donor cell was inserted into the perivitelline space of an enucleated oocyte. The donor cell-oocyte complexes were placed in a solution containing 280 mM mannitol (Nacalai Tesque, Kyoto, Japan), 0.15 mM MgSO₄, 0.01% (w/v) polyvinyl alcohol (PVA) and 0.5 mM HEPES (pH 7.2) and were held between two electrode needles. Membrane fusion was induced using an Electro Cell Fusion Generator (LF201; Nepa Gene, Chiba, Japan) by applying a single pulse of direct-current (DC) (267 V/mm for 20 µs) and pre- and post-pulse alternating currents of 4 V at 1 MHz for 5 s.

The reconstructed embryos were cultured in porcine zygote medium-5 (PZM-5; Research Institute for the Functional Peptides, Yamagata, Japan) supplemented with 4 mg/mL bovine serum albumin for 1 to 1.5 h, followed by electrical activation. For induction of electrical activation, the reconstructed embryos were aligned between two wire electrodes (1.0 mm apart) on a fusion chamber slide filled with the activation solution (280 mM mannitol, 0.05 mM CaCl₂, 0.1 mM MgSO₄ and 0.01% (w/v) PVA). A DC pulse of 150 V/mm was applied for 100 µs using the Electro Cell Fusion Generator. After activation, the reconstructed embryos were cultured in PZM-5 for 3 h in 5 µg/mL CB and 500 nM Scriptaid followed by culture in 500 nM Scriptaid for 12–14 h. To assess their development, the cloned embryos were next cultured in PZM-5 and divided into two groups (SCNT embryos cultured for 1–2 days or 5–6 days). Embryo culture was performed in a humidified atmosphere containing 5% CO₂, 5% O₂, and 90% N₂ at 38.5 °C. After reaching the morula stage, the embryos were cultured in PZM-5 supplemented with 10% FBS.

Crossbred prepubertal gilts weighing 100 to 105 kg were used as recipients of the SCNT embryos after synchronization of oestrus by administration of equine chorionic gonadotropin (eCG, ASKA Pharmaceutical, Tokyo, Japan) and human chorionic gonadotropin (hCG, Kyoritsu Pharmaceutical, Tokyo, Japan). The SCNT embryos at the 1- to 2-cell stage were transferred to the oviduct of the recipients after culture for 1–2 days. After culture for 5–6 days, the SCNT blastocysts were transferred to the uterine horns of the recipients. Embryos were transferred to pigs administered general anaesthesia induced using intramuscular injection of mafoprazine mesylate and thiopental (10 mg/kg, DS Pharma animal Health Co., Ltd., Osaka, Japan), and anaesthesia was maintained by administration of isoflurane gas.

CT analysis. CT analyses of the piglets were performed using a SOMATOM Sensation 16 CT scanner (Siemens AG, Munich, Germany). Piglets were subjected to CT after death. Each specimen was placed in a prone position, and noncontrast CT scans of sections 0.625-mm thick were obtained from vertical axial tomographs acquired at 0.625-mm intervals. Scan settings were 120 kVp, 400 mA, and a tube rotation time of 0.5 s. The grey-scale threshold was set to 75 to separate bone from the surrounding tissue using an adaptive threshold method. Three-dimensional (3D) models of the whole body were based on the 0.625-mm thick CT scan slices generated using Advantage Workstation 4.5 software (GE Healthcare, Waukesha, WI, USA).

Analysis of scoliosis. The spines of pigs potentially suffering from scoliosis were removed during autopsy and analysed using CT. DICOM (Digital Imaging and Communication in Medicine) data were converted to Stereolithography data using AVIZO (FEI Company, Hillsboro, OR, USA). RapidFormORX (Geomagic Inc., Morrisville, NC, USA) was used to determine the 3D coordinates of the upper and lower surfaces of each vertebral body, and these data were used to derive equations for the planes of best fit for each vertebral body. The inner product of the normal unit vectors of the upper and lower planes was calculated, the angle formed by the two planes was determined and the deformity of the lumbar vertebrae was assessed.

Histological analysis. Thoracic aortic tissues were fixed in 10%-neutral buffered formalin solution (Wako Pure Chemical Industries, Osaka, Japan), embedded in paraffin, sectioned, and treated with EVG stain using standard methods. The primary antibodies used were an anti-FBN1 polyclonal antibody (provided by Prof. Tomoyuki Nakamura, Kansai Medical University)⁴⁵ and an anti-FBN2 polyclonal antibody (provided by Dr. Lynn Sakai, Shriner Institute)⁴². The secondary antibody used was an Alexa Fluor 555-conjugated anti-rabbit IgG (Life Technologies), and the nuclei were stained with 4',6-diamidino-2-phenylindole (DAPI). Images were acquired using a confocal microscope with 488- and 543-nm filters (LSM780; Carl Zeiss MicroImaging, Jena, Germany).

References

1. Sakai, L. Y., Keene, D. R. & Engvall, E. Fibrillin, a new 350-kD glycoprotein, is a component of extracellular microfibrils. *J Cell Biol* **103**, 2499–2509 (1986).
2. Robinson, P. N. & Booms, P. The molecular pathogenesis of the Marfan syndrome. *Cell Mol Life Sci* **58**, 1698–1707 (2001).
3. Ramirez, F. & Dietz, H. C. Fibrillin-rich microfibrils: Structural determinants of morphogenetic and homeostatic events. *J Cell Physiol* **213**, 326–330 (2007).
4. Neptune, E. R. *et al.* Dysregulation of TGF-beta activation contributes to pathogenesis in Marfan syndrome. *Nat Genet* **33**, 407–411 (2003).
5. Kaartinen, V. & Warburton, D. Fibrillin controls TGF-beta activation. *Nat Genet* **33**, 331–332 (2003).
6. Dietz, H. C. *et al.* Marfan syndrome caused by a recurrent de novo missense mutation in the fibrillin gene. *Nature* **352**, 337–339 (1991).
7. Lee, B. *et al.* Linkage of Marfan syndrome and a phenotypically related disorder to two different fibrillin genes. *Nature* **352**, 330–334 (1991).
8. Dean, J. C. Marfan syndrome: clinical diagnosis and management. *Eur J Hum Genet* **15**, 724–733 (2007).
9. Canadas, V., Vilacosta, I., Bruna, I. & Fuster, V. Marfan syndrome. Part 1: pathophysiology and diagnosis. *Nat Rev Cardiol* **7**, 256–265 (2010).

10. Pereira, L. *et al.* Targetting of the gene encoding fibrillin-1 recapitulates the vascular aspect of Marfan syndrome. *Nat Genet* **17**, 218–222 (1997).
11. Judge, D. P. *et al.* Evidence for a critical contribution of haploinsufficiency in the complex pathogenesis of Marfan syndrome. *J Clin Invest* **114**, 172–181 (2004).
12. Carta, L. *et al.* Fibrillins 1 and 2 perform partially overlapping functions during aortic development. *J Biol Chem* **281**, 8016–8023 (2006).
13. Lima, B. L. *et al.* A new mouse model for marfan syndrome presents phenotypic variability associated with the genetic background and overall levels of Fbn1 expression. *PLoS One* **5**, e14136 (2010).
14. Cook, J. R. *et al.* Generation of Fbn1 conditional null mice implicates the extracellular microfibrils in osteoprogenitor recruitment. *Genesis* **50**, 635–641 (2012).
15. Yang, D. *et al.* Generation of PPARgamma mono-allelic knockout pigs via zinc-finger nucleases and nuclear transfer cloning. *Cell Res* **21**, 979–982 (2011).
16. Hauschild, J. *et al.* Efficient generation of a biallelic knockout in pigs using zinc-finger nucleases. *Proc Natl Acad Sci USA* **108**, 12013–12017 (2011).
17. Lutz, A. J. *et al.* Double knockout pigs deficient in N-glycolylneuraminic acid and galactose alpha-1,3-galactose reduce the humoral barrier to xenotransplantation. *Xenotransplantation* **20**, 27–35 (2013).
18. Watanabe, M. *et al.* Generation of interleukin-2 receptor gamma gene knockout pigs from somatic cells genetically modified by zinc finger nuclease-encoding mRNA. *PLoS One* **8**, e76478 (2013).
19. Carlson, D. F. *et al.* Efficient TALEN-mediated gene knockout in livestock. *Proc Natl Acad Sci USA* **109**, 17382–17387 (2012).
20. Lee, K. *et al.* Engraftment of human iPS cells and allogeneic porcine cells into pigs with inactivated RAG2 and accompanying severe combined immunodeficiency. *Proc Natl Acad Sci USA* **111**, 7260–7265 (2014).
21. Tan, W. *et al.* Efficient nonmeiotic allele introgression in livestock using custom endonucleases. *Proc Natl Acad Sci USA* **110**, 16526–16531 (2013).
22. Whitworth, K. M. *et al.* Use of the CRISPR/Cas9 system to produce genetically engineered pigs from *in vitro*-derived oocytes and embryos. *Biol Reprod* **91**, 78 (2014).
23. Li, P. *et al.* Efficient generation of genetically distinct pigs in a single pregnancy using multiplexed single-guide RNA and carbohydrate selection. *Xenotransplantation* **22**, 20–31 (2015).
24. Zhou, X. *et al.* Generation of CRISPR/Cas9-mediated gene-targeted pigs via somatic cell nuclear transfer. *Cell Mol Life Sci* **72**, 1175–1184 (2015).
25. Kurome, M. *et al.* Production efficiency and telomere length of the cloned pigs following serial somatic cell nuclear transfer. *J Reprod Dev* **54**, 254–258 (2008).
26. Matsunari, H. *et al.* Transgenic-cloned pigs systemically expressing red fluorescent protein, Kusabira-Orange. *Cloning Stem Cells* **10**, 313–323 (2008).
27. Watanabe, M. *et al.* Production of transgenic cloned pigs expressing the far-red fluorescent protein monomeric Plum. *J Reprod Dev* **61**, 169–177 (2015).
28. Liu, W. O., Oefner, P. J., Qian, C., Odom, R. S. & Francke, U. Denaturing HPLC-identified novel FBN1 mutations, polymorphisms, and sequence variants in Marfan syndrome and related connective tissue disorders. *Genet Test* **1**, 237–242 (1997).
29. Rommel, K., Karck, M., Haverich, A., Schmidtke, J. & Arslan-Kirchner, M. Mutation screening of the fibrillin-1 (FBN1) gene in 76 unrelated patients with Marfan syndrome or Marfanoid features leads to the identification of 11 novel and three previously reported mutations. *Hum Mutat* **20**, 406–407 (2002).
30. Potter, K. J. *et al.* The c.7409G > A (p.Cys2470Tyr) Variant of FBN1: Phenotypic Variability across Three Generations. *Mol Syndromol* **4**, 125–135 (2013).
31. Yang, X. *et al.* Nuclear reprogramming of cloned embryos and its implications for therapeutic cloning. *Nat Genet* **39**, 295–302 (2007).
32. Cao, Z. *et al.* Dynamic reprogramming of 5-hydroxymethylcytosine during early porcine embryogenesis. *Theriogenology* **81**, 496–508 (2014).
33. Bauer, B. K. *et al.* Transcriptional profiling by deep sequencing identifies differences in mRNA transcript abundance in *in vivo*-derived versus *in vitro*-cultured porcine blastocyst stage embryos. *Biol Reprod* **83**, 791–798 (2010).
34. Gjolaj, J. P. *et al.* Spinal deformity correction in Marfan syndrome versus adolescent idiopathic scoliosis: learning from the differences. *Spine (Phila Pa 1976)* **37**, 1558–1565 (2012).
35. Janssen, M. M., de Wilde, R. F., Kouwenhoven, J. W. & Castelein, R. M. Experimental animal models in scoliosis research: a review of the literature. *Spine J* **11**, 347–358 (2011).
36. Nistala, H. *et al.* Differential effects of alendronate and losartan therapy on osteopenia and aortic aneurysm in mice with severe Marfan syndrome. *Hum Mol Genet* **19**, 4790–4798 (2010).
37. Haine, E. *et al.* Muscle and bone impairment in children with Marfan syndrome: correlation with age and FBN1 genotype. *J Bone Miner Res* **30**, 1369–1376 (2015).
38. Hwa, J. *et al.* The natural history of aortic dilatation in Marfan syndrome. *Med J Aust* **158**, 558–562 (1993).
39. Bunton, T. E. *et al.* Phenotypic alteration of vascular smooth muscle cells precedes elastolysis in a mouse model of Marfan syndrome. *Circ Res* **88**, 37–43 (2001).
40. Wu, D., Shen, Y. H., Russell, L., Coselli, J. S. & LeMaire, S. A. Molecular mechanisms of thoracic aortic dissection. *J Surg Res* **184**, 907–924 (2013).
41. Charbonneau, N. L. *et al.* *In vivo* studies of mutant fibrillin-1 microfibrils. *J Biol Chem* **285**, 24943–24955 (2010).
42. Charbonneau, N. L. *et al.* Microfibril structure masks fibrillin-2 in postnatal tissues. *J Biol Chem* **285**, 20242–20251 (2010).
43. National Agriculture and Bio-oriented Research Organization. *Japanese Feeding Standard for Swine*. (Japan Livestock Industry Association, Tokyo) (2005).
44. Doyon, Y. *et al.* Transient cold shock enhances zinc-finger nuclease-mediated gene disruption. *Nat Methods* **7**, 459–460 (2010).
45. Inoue, T. *et al.* Latent TGF-beta binding protein-2 is essential for the development of ciliary zoneule microfibrils. *Hum Mol Genet* **23**, 5672–5682 (2014).

Acknowledgements

We thank Prof. Tomoyuki Nakamura and Dr. Lynn Sakai for providing the anti-fibrillin-1 and anti-fibrillin-2 polyclonal antibodies, respectively; Prof. Eiji Kobayashi, Dr. Takumi Teratani, Dr. Jiro Masubuchi and Prof. Eiji Sugimoto of Jichi Medical University for performing CT; and Dr. Yoshikazu Arai and Dr. Jun Ohgane of Meiji University for performing real-time PCR. Financial support for this study was provided by a Scientific Research Grant (A) (#15H02480 to H.N.) and (B) (#24390357 to M.M.) from the Ministry of Education, Culture, Sports, Science and Technology-Japan; by the Keio Gijyuku Academic Development Funds (to M.M.) and by the Meiji University International Institute for Bio-Resource Research (to H.N.).

Author Contributions

K.U. performed molecular and animal experiments, data acquisition, and analysis and wrote the manuscript. K.W., K.H. and M.K. contributed to data acquisition, data analysis, and interpretation in the orthopaedic research. M.W. established *FBN1* mutant cells lines. K.N. and H.M. generated cloned pigs. T.K. and M.S. contributed to data acquisition and interpretation in the histological analysis. M.N. wrote and revised manuscript. Y.A., O.S. and H.S. contributed to discussion. K.K. conceived the study and contributed to discussion. H.N. conceived and designed the study, contributed to generation of cloned pigs, and edited the manuscript. M.M. conceived and designed the study and contributed to interpretation in the orthopaedic research. All authors approved the final manuscript.

Additional Information

Supplementary information accompanies this paper at <http://www.nature.com/srep>

Competing financial interests: There is potential competing financial interest. H.S. received research grants from Daiichi Sankyo Inc. and Eisai Co. Ltd. These grants did not alter the authors' adherence to all the journal's policies on sharing data and materials.

How to cite this article: Umeyama, K. *et al.* Generation of heterozygous fibrillin-1 mutant cloned pigs from genome-edited foetal fibroblasts. *Sci. Rep.* **6**, 24413; doi: 10.1038/srep24413 (2016).



This work is licensed under a Creative Commons Attribution 4.0 International License. The images or other third party material in this article are included in the article's Creative Commons license, unless indicated otherwise in the credit line; if the material is not included under the Creative Commons license, users will need to obtain permission from the license holder to reproduce the material. To view a copy of this license, visit <http://creativecommons.org/licenses/by/4.0/>

Generation of Interleukin-2 Receptor Gamma Gene Knockout Pigs from Somatic Cells Genetically Modified by Zinc Finger Nuclease-Encoding mRNA

Masahito Watanabe^{1,2}, Kazuaki Nakano¹, Hitomi Matsunari^{1,2}, Taisuke Matsuda¹, Miki Maehara¹, Takahiro Kanai¹, Mirina Kobayashi¹, Yukina Matsumura¹, Rieko Sakai¹, Momoko Kuramoto¹, Gota Hayashida¹, Yoshinori Asano¹, Shuko Takayanagi¹, Yoshikazu Arai¹, Kazuhiro Umeyama^{1,2}, Masaki Nagaya², Yutaka Hanazono^{3,4}, Hiroshi Nagashima^{1,2,4*}

1 Laboratory of Developmental Engineering, Department of Life Sciences, School of Agriculture, Meiji University, Kawasaki, Japan, **2** Meiji University International Institute for Bio-Resource Research (MUIIBR), Kawasaki, Japan, **3** Division of Regenerative Medicine, Center for Molecular Medicine, Jichi Medical University, Tochigi, Japan, **4** CREST, Japan Science and Technology Agency, Tokyo, Japan

Abstract

Zinc finger nuclease (ZFN) is a powerful tool for genome editing. ZFN-encoding plasmid DNA expression systems have been recently employed for the generation of gene knockout (KO) pigs, although one major limitation of this technology is the use of potentially harmful genome-integrating plasmid DNAs. Here we describe a simple, non-integrating strategy for generating KO pigs using ZFN-encoding mRNA. The interleukin-2 receptor gamma (*IL2RG*) gene was knocked out in porcine fetal fibroblasts using ZFN-encoding mRNAs, and *IL2RG* KO pigs were subsequently generated using these KO cells through somatic cell nuclear transfer (SCNT). The resulting *IL2RG* KO pigs completely lacked a thymus and were deficient in T and NK cells, similar to human X-linked SCID patients. Our findings demonstrate that the combination of ZFN-encoding mRNAs and SCNT provides a simple robust method for producing KO pigs without genomic integration.

Citation: Watanabe M, Nakano K, Matsunari H, Matsuda T, Maehara M, et al. (2013) Generation of Interleukin-2 Receptor Gamma Gene Knockout Pigs from Somatic Cells Genetically Modified by Zinc Finger Nuclease-Encoding mRNA. PLoS ONE 8(10): e76478. doi:10.1371/journal.pone.0076478

Editor: Andrew C. Wilber, Southern Illinois University School of Medicine, United States of America

Received July 4, 2013; **Accepted** August 23, 2013; **Published** October 9, 2013

Copyright: © 2013 Watanabe et al. This is an open-access article distributed under the terms of the Creative Commons Attribution License, which permits unrestricted use, distribution, and reproduction in any medium, provided the original author and source are credited.

Funding: This work was supported by the Core Research for Evolutional Science and Technology (CREST) of the Japan Science and Technology Agency and by the Meiji University International Institute for Bio-Resource Research (MUIIBR). The funders had no role in study design, data collection and analysis, decision to publish, or preparation of the manuscript.

Competing Interests: The authors have declared that no competing interests exist.

* E-mail: hnagas@isc.meiji.ac.jp

Introduction

Pigs have attracted attention as large experimental animals capable of providing valuable information that is highly extrapolatable to humans due to their anatomical, physiological, and hematological features [1–5]. To date, pig models of various human diseases, such as cystic fibrosis [6], diabetes mellitus [7,8], Alzheimer's disease [9], and retinitis pigmentosa [10], have been created. In addition, research on the use of genetically modified pigs as organ/tissue donors for xenotransplantation into humans is advancing [11,12]. In fact, encapsulated porcine islets of Langerhans have been transplanted into humans and are now under clinical trials to assess their safety and efficacy for curing type I diabetes mellitus [13].

The knockout (KO) of endogenous genes is a useful tool for analyses of gene function and the production of animal models that mimic human diseases. A variety of gene KO mice have been generated using embryonic stem (ES) cells genetically modified by homologous recombination (HR). As authentic ES cells are not available in pigs, HR using somatic cells has been employed to generate gene KO pigs in combination with somatic cell nuclear transfer (SCNT) technology. However, the low efficiency (frequency, 10^{-6} to 10^{-8}) of HR for mammalian cultured cells

hinders the generation of KO pigs [14–16], and the generation of KO pigs through HR therefore remains limited.

One new technique uses zinc finger nucleases (ZFNs) to knock out endogenous genes and is expected to overcome the inefficiency and complexity of HR in mammals [17]. Engineered ZFNs are artificial restriction enzymes comprised of a zinc finger DNA-binding domain and a DNA cleavage domain [18]. We previously were the first to demonstrate that gene KO in primary porcine fetal fibroblasts *in vitro* was possible using ZFNs [19], and somatic cells that were genetically modified by ZFNs were shown to be capable of producing gene KO pigs after SCNT [20–23]. In these studies, the ZFN-encoding plasmid DNA was introduced into somatic cells or the nuclear donor cells for SCNT. However, plasmid DNA can also be integrated into the genome of cells, which may result in the disruption of endogenous genes and the constitutive expression of ZFNs. This drawback of plasmid DNA can be eliminated by the use of ZFN-encoding mRNA, which cannot be inserted into the host genome. Gene KO using ZFN-encoding mRNAs in rodents has been performed via direct injection into the fertilized eggs [24–26], although the generation of KO piglets using ZFN-encoding mRNA has yet to be reported.

The present study sought to investigate whether ZFN-encoding mRNAs can be used to generate gene KO pigs. We chose the

interleukin-2 receptor gamma (*IL2RG*) gene on the X-chromosome of male cells as a target gene to be knocked out. *IL2RG* encodes the common gamma chain (γ_c), and mutations in *IL2RG* lead to X-linked severe combined immunodeficiency (XSCID), which is characterized by profound defects in cellular and humoral immunity in humans [27,28]. Furthermore, knockout of *IL2RG* was previously shown to give rise to the XSCID phenotype in male pigs [29]. We therefore applied ZFN-encoding mRNA to knock out *IL2RG* in male porcine fibroblast cells, which are capable of supporting the development to live offspring after SCNT. Here, we show that an endogenous gene in porcine primary cultured cells could be knocked out using ZFN-encoding mRNAs, thereby allowing the efficient production of a gene KO pig by means of somatic cell cloning.

Results

Design of ZFNs and isolation of *IL2RG* KO cells

Similar to *IL2RG* in humans, mice, and rats, porcine *IL2RG* is found on the X chromosome and consists of 8 exons [30]. In this study, we constructed a ZFN that targets exon 1 of porcine *IL2RG*. This pair (right and left) of ZFNs contains 4 zinc finger proteins each, and both the right and left ZFNs recognize a target sequence of 24 bp (Figure 1A). *IL2RG* KO cells were generated via the electroporation of ZFN-encoding mRNAs into porcine male fetal fibroblasts with transient cold shock treatment at 32°C for 3 d [31]. No visible morphological abnormalities were detected in the fetal fibroblasts following the introduction of mRNA and transient cold shock treatment. Of the 192 single cell-derived cell lines obtained by limiting dilution, 1 cell line (1/192, 0.5%) with a ZFN-induced mutation was established, and this cell line (#98, Figure 1B) was used as the nuclear donor for SCNT. DNA sequence analyses showed that these cells carried both a 3-bp substitution and an 86-bp deletion spanning the major transcription start point and the start codon (ATG) of porcine *IL2RG*, indicating that this mutation was likely to disrupt *IL2RG* function. Sufficient numbers of KO cells were prepared for SCNT after culture for 3 weeks.

Production and analysis of *IL2RG* KO cloned pigs

First, the developmental competence of the SCNT embryos reconstructed with the *IL2RG* KO cells was examined *in vitro*. Of the 403 SCNT embryos produced in duplicated experiments, 237 (58.8%) developed into blastocysts (Table 1). This blastocyst formation rate was comparable to those reported in our previous studies [32]. Second, 199 blastocysts (Figure 2A) obtained by SCNT were subjected to transfer to 2 estrus synchronized recipient gilts (P177 and P178; Table 1). Pregnancy was confirmed in both gilts at 39 d of gestation. On day 113 of gestation, 4 male cloned pigs were obtained from 1 recipient (P177) via cesarean section (Figure 2B). The body weight and length of the 4 piglets ranged from 0.56 to 1.16 kg and 22 to 28 cm, respectively. The other recipient (P178) miscarried at 46 d of gestation.

PCR genotyping and DNA sequence analyses of the 4 cloned pigs showed that all 4 pigs had the same mutation as the nuclear donor cells (3-bp substitution and 86-bp deletion; Figure 2C and D). Western blot analyses further showed that all 4 pigs lacked the *IL2RG* protein (Figure 2E).

Phenotypic characterization of *IL2RG* KO pigs

Gross anatomical analysis revealed that all 4 *IL2RG* KO pigs completely lacked thymuses (Figure 3A, B). Histological analysis of the spleens clearly showed the presence of lymphocytes in the white pulp of the peripheral lymphoid sheath tissue (PALS) in

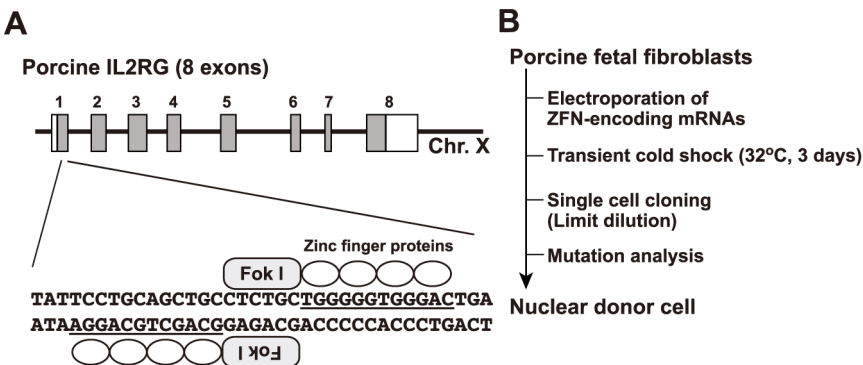
wild-type (WT) pigs (Figure 3C), whereas the *IL2RG* KO pigs showed very few or no lymphocytes in the PALS (Figure 3D). Embryonic hematopoiesis in the red pulp was strong in both WT and *IL2RG* KO pigs (data not shown). The lymphocyte counts in the peripheral blood of the WT and *IL2RG* KO pigs were $15.7 \pm 2.2 \times 10^2/\mu\text{l}$ and $6.5 \pm 3.0 \times 10^2/\mu\text{l}$, respectively, indicating a significant reduction in the lymphocyte number in *IL2RG* KO pigs ($P < 0.01$; Figure 3E).

Flow cytometric analyses of the peripheral blood (Figure 4A) showed that the number of $\text{CD}3^+$ T cells in *IL2RG* KO pigs ($0.3\% \pm 0.1\%$) was drastically lower than that in WT pigs ($74.0\% \pm 10.2\%$; $P < 0.0001$). In addition, *IL2RG* KO pigs lacked $\text{CD}3^+\text{CD}4^+$ and $\text{CD}3^+\text{CD}8^+$ T cells. The number of NK cells (monocyte/granulocyte $^-$, $\text{CD}3^-$, and $\text{CD}16^+$) was also notably lower in *IL2RG* KO pigs than WT pigs (*IL2RG* KO, $0.9\% \pm 0.2\%$ vs. WT, $8.1 \pm 4.5\%$; $P = 0.004$), although the B cell population ($\text{CD}3^-$ and $\text{CD}45\text{RA}^+$) in *IL2RG* KO pigs was observed to be the same as that in WT pigs. As observed in the peripheral blood, the numbers of splenic T cells (*IL2RG* KO, $0.2\% \pm 0.1\%$ vs. WT, $28.1\% \pm 10.9\%$; $P < 0.0001$) and NK cells (*IL2RG* KO, $0.8\% \pm 0.3\%$ vs. WT, $3.9\% \pm 0.8\%$; $P = 0.0001$) were significantly reduced in *IL2RG* KO pigs (Figure 4B). Thus, an almost complete lack of T and NK cells was observed in the *IL2RG* KO pigs, which is similar to human XSCID patients.

Discussion

In rodents, the microinjection of ZFN-encoding mRNA into fertilized eggs has been used for the creation of gene KO animals, mainly due to its simplicity. However, the drawbacks of this microinjection method include inefficiency and the occurrence of mutation mosaicism [24]. The transfer of mRNA-injected eggs into recipient females gives rise to both non-mutant and mutant offspring, and the generation of mutants results in undesired mutations that are meaningless with regard to the traits of the gene KO animals. Mutation mosaicism can result from sustained ZFN activity during later embryogenesis or the re-cleavage of the already-modified alleles [33,34]. Individuals with the desired mutation can be selected after crossbreeding with WT animals. Such a breeding process, however, requires enormous time, labor, and costs in large animals such as pigs, which have longer gestation intervals than rodents. We therefore applied the gene KO procedure using SCNT for the generation of *IL2RG* KO pigs in the present study. With this method, nuclear donor cells could be examined *in vitro* for the induced mutations prior to the production of cloned animals by SCNT [2]. Thus, the wasteful production of undesired animals can be avoided. To our knowledge, this study is the first to demonstrate the generation of cloned pigs from gene KO cells prepared using ZFN-encoding mRNA.

For the generation of gene KO pigs by somatic cell cloning, HR has traditionally been used to knock out a target gene in nuclear donor cells [11,12,29]. In HR, an antibiotic-based cell selection is performed to obtain KO cells; however, several issues arise, including (1) the insertion of an antibiotic cassette into the host genome using targeting vectors, (2) the senescence or exhaustion of nuclear donor cells caused by the prolonged culture associated with antibiotic selection, and (3) the unavoidable contamination of non-targeted cells despite the positive–negative screening [29,35–37]. Therefore, a re-cloning process, namely repeated nuclear transfer, is often necessary to obtain KO offspring [38,39]. In the re-cloning process, fetuses are collected after the first round of SCNT and embryo transfer, and these first-round cloned fetuses can be analyzed for gene KO status. The establishment of primary



C

Figure 1. Design of ZFNs targeting the pig *IL2RG* gene and isolation of nuclear donor cells. (A) Schematic representation of ZFNs binding to pig *IL2RG*. The coding and untranslated regions are indicated by gray and white boxes, respectively. A ZFN consists of a nuclease domain (Fok I) and a DNA-binding domain (zinc finger proteins), and the recognition sequences of the zinc finger proteins are underlined. (B) Flow chart for the isolation of nuclear donor cells (clone #98) for SCNT. (C) ZFN-induced mutation in cell clone #98. The upper and lower sequences represent the WT and clone #98 sequence of *IL2RG*, respectively. The deletion mutation and nucleotide substitution in clone #98 are indicated by a hyphen and black box, respectively. The initiation codon of *IL2RG* is shown in a dotted box. The ZFN-binding and ZFN-cleavage sites are double-underlined and boxed, respectively. The major transcription initiation site is indicated with a circle.
doi:10.1371/journal.pone.0076478.g001

culture cells from the gene KO fetus requires obtaining rejuvenated nuclear donor cells for the next round of SCNT. Using these rejuvenated cells, the antibiotic cassette can be

excised, provided that the proper site-specific recombinase technology, such as Cre-*loxP* recombination, was incorporated [40].

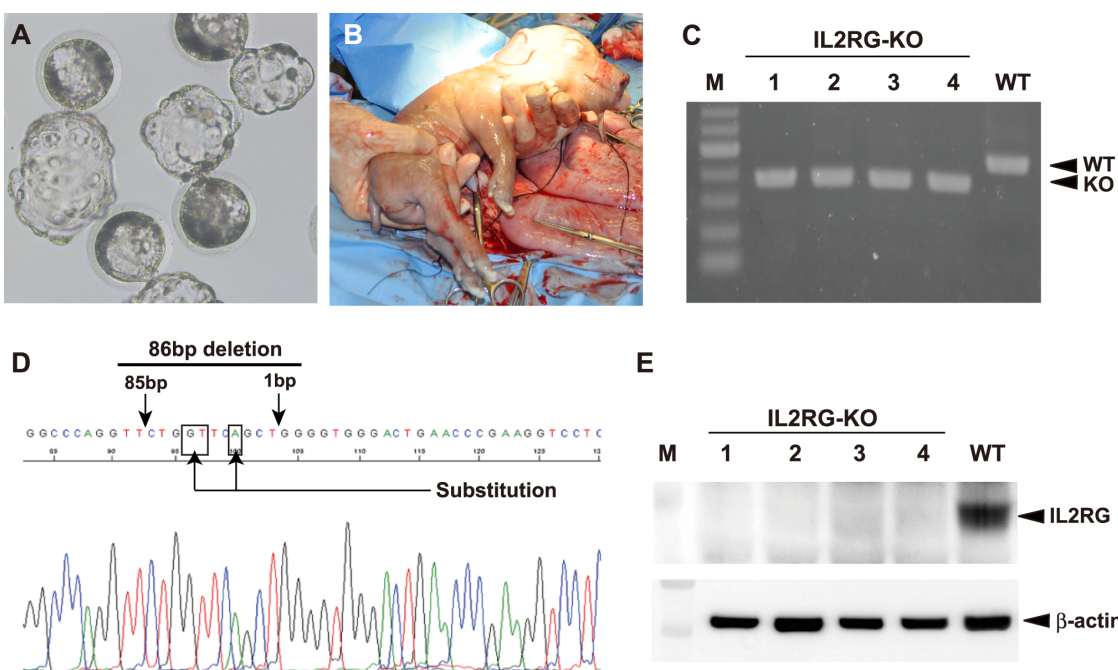


Figure 2. Generation and analysis of *IL2RG* KO pigs. (A) Cloned blastocysts transferred to recipient gilts. (B) Cloned *IL2RG* KO pig delivered by cesarean section at 113 d of gestation. (C) PCR genotyping for the 4 cloned piglets obtained. M: DNA marker. (D) The DNA sequence analysis of *IL2RG* in a cloned pig. The arrows and boxes indicate the same mutation as that of the nuclear donor cell (clone #98). (E) Western blot for *IL2RG* protein in the spleens of *IL2RG* KO pigs. β -actin was used as a loading control. M: protein standard marker.
doi:10.1371/journal.pone.0076478.g002

Table 1. *in vitro* development of SCNT embryos and production of *IL2RG* KO pigs.

<i>in vitro</i> development of reconstructed SCNT embryos		
SCNT embryos reconstructed	403	
Normally cleaved embryos on day 2	151 (71.9%)	
Blastocyst-stage embryos on day 5	237 (58.8%)	
Production of <i>IL2RG</i> KO pigs		
Recipient	P177	P178
Blastocysts transferred ^a	100	99
Pregnancy	+	+
Cloned fetuses obtained	4 (4.0%)	- (miscarried) ^b

^aDay 5–6 embryos.

^b46 d of gestation.

doi:10.1371/journal.pone.0076478.t001

In contrast, ZFN-encoding mRNAs can generate gene KO cells without antibiotic selection. In fact, sufficient numbers of nuclear donor cells for SCNT can be obtained in a short period of time (approximately 3 weeks). Moreover, the *IL2RG*-KO cells generated by the ZFN-encoding mRNAs in this study allowed for the direct production of full-term cloned fetuses without rejuvenation of the nuclear donor cells and subsequent re-cloning. As a result, we obtained full-term cloned fetuses within 6 months, including the period spent establishing the KO cells, whereas the HR method requires an average of 12 to 18 months to obtain KO animals. An additional advantage of ZFN-encoding mRNAs is transient ZFN expression, which reduces the incidence of off-target mutations [41]. Off-target events are a potential limitation of the ZFN technique [26,42,43], although the introduction of ZFN-encoding mRNAs leads to the immediate translation of ZFNs in the cytoplasm without the risk of genomic integration, which could disrupt endogenous genes. Carlson et al. recently

generated KO pigs using TALEN-encoding mRNA [44]. Based on these collective results, we believe that it is important to compare the efficiencies of ZFN- and TALEN-mRNA in generating KO pigs.

A marked decrease in the number of T and B cells has been reported in XSCID mice [45,46] and rats [24]. In human XSCID patients, although the number of T and NK cells is significantly decreased, the number of B cells remains normal or is occasionally increased [28,47]. Thus, the phenotypes of rodent XSCID models do not necessarily mimic the conditions of human XSCID. In contrast, the *IL2RG* KO pigs obtained in this study lacked T and NK cells but showed normal B cell populations, and identical phenotypic characteristics were shown in a previous report in which XSCID pigs were generated through HR [29]. Thus, *IL2RG* KO pigs are considered to be an accurate model that mimics human XSCID.

Opportunistic infections in XSCID animals after birth are unavoidable under conventional housing conditions. We therefore used the full-term *IL2RG* KO pig fetuses recovered via cesarean section (113 d of gestation) for our analyses to avoid any changes due to infections.

In conclusion, this study presents a simple, non-integrating strategy for generating KO pigs using ZFN-encoding mRNA, which successfully generated *IL2RG* KO pigs via the SCNT method in a short period of time. The combination of ZFN-encoding mRNA with SCNT provides a robust method for generating KO pigs without genomic integration. Moreover, the resulting *IL2RG* KO pigs showed a phenotype similar to that of human XSCID. Although further characterization is required, these findings represent the first step toward developing a porcine SCID model, and we believe that this *IL2RG* KO pig model will greatly contribute not only to cancer and stem cell research but also to preclinical evaluations of the transplantation of pluripotent stem cells, such as iPS cells.

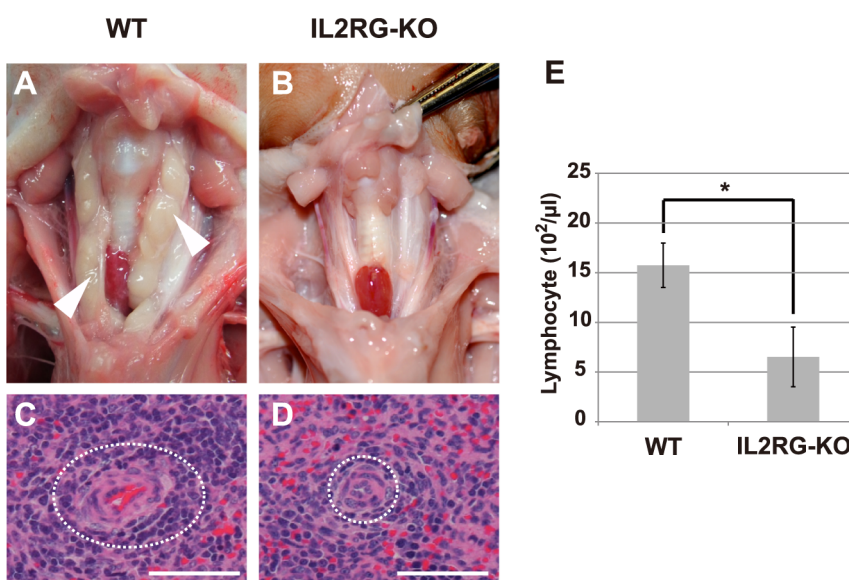


Figure 3. Phenotypes of *IL2RG* KO pigs. (A, B) The thymic phenotype in WT and *IL2RG* KO pigs. The white arrowheads indicate normal thymuses in WT pigs. (C, D) Histological analysis of the spleens of WT and *IL2RG* KO pigs. The white pulp of the spleen is indicated by a dotted white circle. Bar = 100 μm . (E) The proportion of lymphocytes in the peripheral blood (PB) of WT and *IL2RG* KO pigs. The data represent the means \pm SD values for 4 pigs. The asterisk indicates a statistically significant difference ($P<0.01$) between the values for WT and *IL2RG* KO pigs ($n=4$). doi:10.1371/journal.pone.0076478.g003

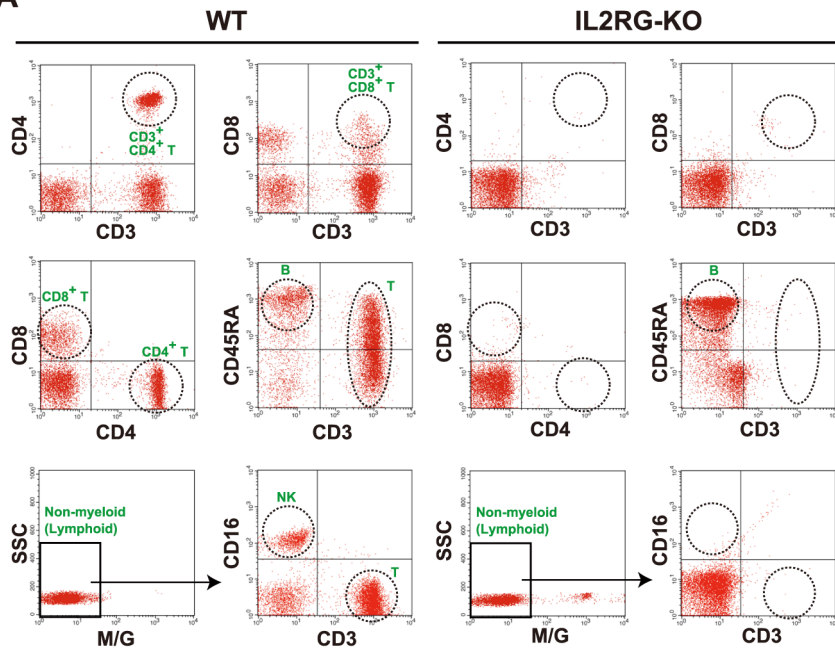
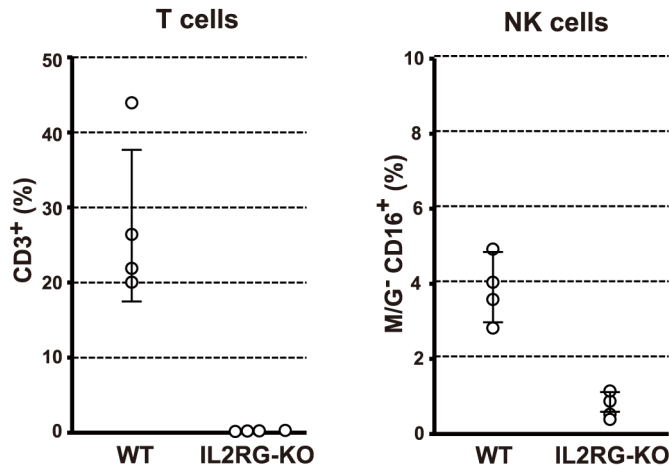
A**B**

Figure 4. Flow cytometric analysis of mononuclear cells in IL2RG KO pigs. (A) Flow cytometric analysis of T, B, and NK cells in the peripheral blood of IL2RG KO pigs. The dot plots show CD3, CD4, and CD8 cells for the demarcation of T cell subpopulations and CD3, CD45RA, and CD16 (in the non-myeloid fraction, i.e., monocyte/granulocyte (M/G)-negative) cells for the differentiation of T cell, B cell, and NK cell subpopulations in the peripheral blood, respectively. (B) The proportion of T (CD3⁺) and NK (M/G⁻, CD3⁻, CD16⁺) cells among the mononuclear cells in the spleens of IL2RG KO pigs. The data represent the mean ± SD values of the 4 pigs obtained.

doi:10.1371/journal.pone.0076478.g004

Materials and Methods

Animal care and chemicals

All of the animal experiments in this study were approved by the Institutional Animal Care and Use Committee of Meiji University (IACUC10-0004). All chemicals were purchased from the Sigma-Aldrich Chemical Co. (MO, USA) unless otherwise indicated.

Design of ZFNs and mRNA preparation

Custom ZFN plasmids for pig *IL2RG* were obtained from Toolgen Inc. The design and validation of these ZFNs was performed by Toolgen Inc (Seoul, South Korea). The constructed ZFNs were designed to target the sequence of exon 1 in the pig *IL2RG* gene. Each of the ZFNs had 4 zinc finger domains

recognizing 12 bases (Figure 1). For the production of ZFN-encoding mRNA, each of the ZFN plasmids was digested with the restriction enzyme Xho I. The linearized plasmids were then purified with phenol/chloroform to generate a high-quality DNA template for *in vitro* transcription. Capped ZFN mRNA was produced from the linearized DNA template via *in vitro* transcription using a MessageMAX T7 ARCA-Capped Message Transcription Kit (Cambio, Cambridge, UK). A poly(A) tail was then added to each mRNA by polyadenylation using the Poly(A) Polymerase Tailing Kit (Cambio). The poly(A)-tailed ZFN-encoding mRNA was then purified using a spin column with the MEGAclear Kit (Life Technologies, CA, USA) and finally resuspended in RNase-free water at 400 ng/ μl.

Isolation of *IL2RG* KO cells and culture conditions

A primary culture of porcine fetal fibroblast cells (male line) was used as the progenitor line for the isolation of *IL2RG* KO cells. The fibroblast cells and their derivatives (KO cells) were seeded onto type I collagen-coated dishes or plates (Asahi Glass, Tokyo, Japan) and cultured in MEM α (Life Technologies) supplemented with 15% FBS (Nichirei Bioscience, Tokyo, Japan) and 1× antibiotic-antimycotic solution (Life Technologies) in a humidified atmosphere containing 5% CO₂ at 37°C. The fetal fibroblasts were cultured to 70–90% confluence, washed twice with D-PBS(−) (Life Technologies), and treated with 0.05% trypsin-EDTA (Life Technologies) to isolate and collect the cells. The cells (4×10⁵) were then suspended in 40 µl of R buffer (supplied as part of the Neon Transfection System, Life Technologies), and 2 µl of ZFN-encoding mRNA solution (400 ng/ µl) was added. The cells were then electroporated under the following conditions: pulse voltage, 1,100 V; pulse width, 30 ms; and pulse number, 1 (program #6). Following electroporation, the cells were cultured at 32°C for 3 d (transient cold shock) first without antibiotics in the medium described above for 24 h and then with antibiotics in the medium [31]. For recovery after the transient cold shock treatment, the cells were cultured at 37°C until they approached confluence, and then limiting dilution was performed to obtain single cell-derived clones in five 96-well plates. At 12 d after limiting dilution, cells at relatively high confluency (>50%) in each well were selected and divided for further culture and mutation analysis. The cells at low confluency (~50%) after limiting dilution were not used in further experiments.

Analysis of ZFN-induced mutations in nuclear donor cells and cloned fetuses

The target region of IL2RG-ZFNs was amplified by direct PCR from the cell clones using MightyAmp DNA polymerase (Takara Bio, Shiga, Japan) and the corresponding primers (5'-ATAGTGGTGTCACTGATTGAGC and 5'-TACGAACT-GACTTATGACTTACC). Nested PCR was then performed using PrimeSTAR HS DNA polymerase (Takara Bio) and the appropriate primers (5'-ATACCCAGCTTCGTCTCTGC and 5'-TTCCAGAATTCTATACGACC). Subsequently, the PCR fragment including the ZFN target region was examined using the sequencing primer 5'-AGCCTGTGTCA TAGCATAAC, the BigDye Terminator Cycle Sequencing Kit, and an ABI PRISM 3100 Genetic Analyzer (Life Technologies). For analysis of the mutation in cloned fetuses, genomic DNA was extracted from the tail biopsies of fetuses using a DNeasy Tissue and Blood Kit (QIAGEN, Hilden, Germany), and then PCR genotyping and DNA sequencing were performed as described above. All new sequence data is deposited in DDBJ/EMBL/GenBank (AB846644-AB846648).

SCNT and embryo transfer

SCNT was performed as described previously with slight modifications [32]. Briefly, *in vitro*-matured oocytes containing the first polar body were enucleated via the gentle aspiration of the polar body and the adjacent cytoplasm using a beveled pipette in 10 mM HEPES-buffered Tyrode lactose medium containing 0.3% (w/v) polyvinylpyrrolidone (PVP), 0.1 µg/ml demecolcine, 5 µg/ml cytochalasin B (CB), and 10% FBS. Fibroblasts (clone #98) were used as nuclear donors following cell cycle synchronization via serum starvation for 2 d. A single donor cell was inserted into the perivitelline space of an enucleated oocyte. The donor cell-oocyte complexes were placed in a solution of 280 mM mannitol (Nacalai Tesque, Kyoto, Japan) (pH 7.2) containing 0.15 mM

MgSO₄, 0.01% (w/v) PVA, and 0.5 mM HEPES and were held between 2 electrode needles. Membrane fusion was induced with a somatic hybridizer (LF201; NEPA GENE, Chiba, Japan) by applying a single direct-current (DC) pulse (200 V/mm, 20 µs) and a pre- and post-pulse alternating current (AC) field of 5 V at 1 MHz for 5 s. The reconstructed embryos were cultured in NCSU23 medium supplemented with 4 mg/ml BSA for 1 to 1.5 h, followed by electrical activation. The reconstructed embryos were then washed twice in an activation solution containing 280 mM mannitol, 0.05 mM CaCl₂, 0.1 mM MgSO₄, and 0.01% (w/v) PVA and were aligned between 2 wire electrodes (1.0 mm apart) of a fusion chamber slide filled with the activation solution. A single DC pulse of 150 V/mm was applied for 100 µs using an electrical pulsing machine (Multiporator; Eppendorf, Hamburg, Germany). After activation, the reconstructed embryos were transferred into PZM5 supplemented with 5 µg/ml CB and 500 nM Scriptaid for 3 h. The embryos were then transferred into PZM5 supplemented with Scriptaid and further cultured for 12 to 14 h. After incubation, the embryos were further cultured in PZM5, and the dish was maintained under a humidified atmosphere of 5% CO₂, 5% O₂, and 90% N₂ at 38.5°C. Beyond the morula stage, the embryos were cultured in PZM5 supplemented with 10% FBS.

Crossbred (Large White/Landrace × Duroc) prepubertal gilts weighing 100 to 105 kg were used as recipients of the SCNT embryos. The gilts were given a single intramuscular injection of 1,000 IU of eCG to induce estrus. Ovulation was induced by an intramuscular injection of 1,500 IU of hCG (Kawasaki Pharmaceutical, Kanagawa, Japan) that was given 66 h after the injection of eCG. The SCNT embryos cultured for 5 to 6 d were surgically transferred into the oviducts of the recipients approximately 146 h after hCG injection.

Western blot analysis

After the *IL2RG* KO and age-matched WT pigs were sacrificed, their dissected spleens were homogenized in RIPA buffer (Thermo Scientific, MA, USA) with a protease inhibitor cocktail (Nacalai Tesque) and subjected to centrifugation, and the supernatants were collected. The protein concentrations of the samples were quantified using a DC protein assay (Bio-Rad, CA, USA) based on the Lowry method. Approximately 40 µg of protein from the spleen extracts was subjected to 10% SDS-PAGE and transferred by electroblotting to a Hybond-P PVDF membrane (GE Healthcare Bio-Sciences, NJ, USA). The membranes were blocked for 30 min at room temperature with Blocking One (Nacalai Tesque). After blocking, the membranes were incubated with an anti-IL2RG antibody (1:200 dilution; Santa Cruz Biotechnology, CA, USA) for 1 h at room temperature and were subsequently incubated with HRP-conjugated anti-rabbit IgG antibody (1:5,000 dilution; Santa Cruz Biotechnology) for 1 h at room temperature. The blot was developed using ECL Western Blotting Detection Reagents (GE Healthcare Bio-Sciences). The signal was detected and imaged with an ImageQuant LAS-4000 system (GE Healthcare Bio-Sciences).

Flow cytometric analysis

Peripheral blood mononuclear cells were harvested from the whole blood and spleens of *IL2RG* KO pigs using the erythrocyte lysis solution PharmLyse (Becton Dickinson, BD, NJ, USA), and 1×10⁶ cells were incubated with mouse anti-pig CD3e (Abcam, Cambridge, UK), CD4a (BD), CD8a (BD), CD16 (AbDSerotec, NC, USA), CD45RA (AbDSerotec), and monocyte and granulocyte (M/G; Abcam) antibodies for 30 min at room temperature. After incubation, the cell suspension was washed and resuspended

with PBS (−) supplemented with 1% FBS (w/v). The cell populations isolated from the peripheral blood and spleens of *IL2RG*-KO pigs were evaluated using a FACSCalibur flow cytometer (BD) equipped with a 488-nm argon laser. The cell debris and aggregates were gated out of the analysis using bivariate, forward/side scatter (FSC/SSC) parameters. In all analyses, the virtual lymphocyte population was gated, and the gated 1×10^4 events per sample were acquired and analyzed using CELLQuest Pro software (BD).

Histological analysis

After the *IL2RG* KO and age-matched WT pigs were sacrificed, their dissected spleens were fixed in 10% neutral buffered formalin

solution (Wako Pure Chemical Industries, Osaka, Japan), embedded in paraffin, sectioned, and stained with hematoxylin and eosin using standard methods.

Acknowledgments

We acknowledge Mr. Hiroshi Kadoi (Kadoi Ltd.) for technical help.

Author Contributions

Conceived and designed the experiments: HN. Performed the experiments: MW KN HM TM MM TK M. Kobayashi YM RS M. Kuramoto GH Y. Asano ST Y. Arai. Analyzed the data: MW KN KU. Wrote the paper: MW MN HN. Final approval of the manuscript: MN YH HN.

References

1. Aigner B, Renner S, Kessler B, Klymiuk N, Kurome M, et al. (2010) Transgenic pigs as models for translational biomedical research. *J Mol Med* 88: 653–664.
2. Kue WA, Niemann H (2004) The contribution of farm animals to human health. *Trends Biotechnol* 22: 286–294.
3. Vajta G, Gjerris M (2006) Science and technology of farm animal cloning: state of the art. *Anim Reprod Sci* 92: 211–230.
4. Lunney JK (2007) Advances in swine biomedical model genomics. *Int J Biol Sci* 3: 179–184.
5. Matsunari H, Nagashima H (2009) Application of genetically modified and cloned pigs in translational research. *J Reprod Dev* 55: 225–230.
6. Rogers CS, Stoltz DA, Meyerholz DK, Ostedgaard LS, Rokhlina T, et al. (2008) Disruption of the CPT1 gene produces a model of cystic fibrosis in newborn pigs. *Science* 321: 1837–1841.
7. Umeyama K, Watanabe M, Saito H, Kurome M, Tohi S, et al. (2009) Dominant-negative mutant hepatocyte nuclear factor 1alpha induces diabetes in transgenic-cloned pigs. *Transgenic Res* 18: 697–706.
8. Renner S, Fehlings C, Herbach N, Hofmann A, von Waldthausen DC, et al. (2010) Glucose intolerance and reduced proliferation of pancreatic beta-cells in transgenic pigs with impaired glucose-dependent insulinotropic polypeptide function. *Diabetes* 59: 1228–1238.
9. Kragh PM, Nielsen AL, Li J, Du Y, Lin L, et al. (2009) Hemizygous minipigs produced by random gene insertion and handmade cloning express the Alzheimer's disease-causing dominant mutation APPsw. *Transgenic Res* 18: 545–558.
10. Ross JW, Fernandez de Castro JP, Zhao J, Samuel M, Walters E, et al. (2012) Generation of an inbred miniature pig model of retinitis pigmentosa. *Invest Ophthalmol Vis Sci* 53: 501–507.
11. Dai Y, Vaught TD, Boone J, Chen SH, Phelps CJ, et al. (2002) Targeted disruption of the alpha1,3-galactosyltransferase gene in cloned pigs. *Nat Biotechnol* 20: 251–255.
12. Lai L, Kolber-Simonds D, Park KW, Cheong HT, Greenstein JL, et al. (2002) Production of alpha1,3-galactosyltransferase knockout pigs by nuclear transfer cloning. *Science* 295: 1089–1092.
13. Elliott RB, Escobar L, Tan PL, Muzina M, Zwain S, et al. (2007) Live encapsulated porcine islets from a type 1 diabetic patient 9.5 yr after xenotransplantation. *Xenotransplantation* 14: 157–161.
14. Porter AC, Itzhaki JE (1993) Gene targeting in human somatic cells. Complete inactivation of an interferon-inducible gene. *Eur J Biochem* 218: 273–281.
15. Brown JP, Wei W, Sedivy JM (1997) Bypass of senescence after disruption of p21cip1/WAF1 gene in normal diploid human fibroblasts. *Science* 277: 831–834.
16. van Nierop GP, de Vries AA, Holkers M, Vrijen KR, Goncalves MA (2009) Stimulation of homology-directed gene targeting at an endogenous human locus by a nicking endonuclease. *Nucleic Acids Res* 37: 5725–5736.
17. Geurts AM, Cost GJ, Freyvert Y, Zeitzer B, Miller JC, et al. (2009) Knockout rats via embryo microinjection of zinc-finger nucleases. *Science* 325: 433.
18. Kim YG, Cha J, Chandrasegaran S (1996) Hybrid restriction enzymes: zinc finger fusions to Fok I cleavage domain. *Proc Natl Acad Sci U S A* 93: 1156–1160.
19. Watanabe M, Umeyama K, Matsunari H, Takayanagi S, Haruyama E, et al. (2010) Knockout of exogenous EGFP gene in porcine somatic cells using zinc-finger nucleases. *Biochem Biophys Res Commun* 402: 14–18.
20. Whyte JJ, Zhao J, Wells KD, Samuel MS, Whitworth KM, et al. (2011) Gene targeting with zinc-finger nucleases to produce cloned eGFP knockout pigs. *Mol Reprod Dev* 78: 2.
21. Hausschild J, Petersen B, Santiago Y, Queisser AL, Carnwath JW, et al. (2011) Efficient generation of a biallelic knockout in pigs using zinc-finger nucleases. *Proc Natl Acad Sci U S A* 108: 12013–12017.
22. Li P, Estrada JL, Burlak C, Tector AJ (2012) Biallelic knockout of the alpha-1,3 galactosyltransferase gene in porcine liver-derived cells using zinc finger nucleases. *J Surg Res* 181: e39–45.
23. Yang D, Yang H, Li W, Zhao B, Ouyang Z, et al. (2011) Generation of PPARgamma mono-allelic knockout pigs via zinc-finger nucleases and nuclear transfer cloning. *Cell Res* 21: 979–982.
24. Mashimo T, Takizawa A, Voigt B, Yoshimi K, Hiai H, et al. (2010) Generation of knockout rats with X-linked severe combined immunodeficiency (X-SCID) using zinc-finger nucleases. *PLoS One* 5: e8870.
25. Carberry ID, Ji D, Harrington A, Brown V, Weinstein EJ, et al. (2010) Targeted genome modification in mice using zinc-finger nucleases. *Genetics* 186: 451–459.
26. Cui X, Ji D, Fisher DA, Wu Y, Briner DM, et al. (2011) Targeted integration in rat and mouse embryos with zinc-finger nucleases. *Nat Biotechnol* 29: 64–67.
27. Noguchi M, Yi H, Rosenblatt HM, Filipovich AH, Adelstein S, et al. (1993) Interleukin-2 receptor gamma chain mutation results in X-linked severe combined immunodeficiency in humans. *Cell* 73: 147–157.
28. Buckley RH (2004) Molecular defects in human severe combined immunodeficiency and approaches to immune reconstitution. *Annu Rev Immunol* 22: 625–655.
29. Suzuki S, Iwamoto M, Saito Y, Fuchimoto D, Sembon S, et al. (2012) II2rg Gene-Targeted Severe Combined Immunodeficiency Pigs. *Cell Stem Cell* 10: 753–758.
30. Honma D, Uenishi H, Hiraiwa H, Watanabe S, Tang W, et al. (2003) Cloning and characterization of porcine common gamma chain gene. *J Interferon Cytokine Res* 23: 101–111.
31. Doyon Y, Choi VM, Xia DF, Vo TD, Gregory PD, et al. (2010) Transient cold shock enhances zinc-finger nuclease-mediated gene disruption. *Nat Methods* 7: 459–460.
32. Matsunari H, Watanabe M, Umeyama K, Nakano K, Ikezawa Y, et al. (2012) Cloning of homozygous α 1,3-galactosyltransferase gene knock-out pigs by somatic cell nuclear transfer. In: Miyagawa S, editor. *Xenotransplantation*. Rijeka, Croatia: InTech. pp. 37–54.
33. Tesson L, Usa C, Menoret S, Leung E, Niles BJ, et al. (2011) Knockout rats generated by embryo microinjection of TALENs. *Nat Biotechnol* 29: 695–696.
34. Sung YH, Baek JY, Kim DH, Jeon J, Lee J, et al. (2013) Knockout mice created by TALEN-mediated gene targeting. *Nat Biotechnol* 31: 23–24.
35. Forsberg EJ, Strelenko NS, Augenstein ML, Bethausser JM, Childs LA, et al. (2002) Production of cloned cattle from in vitro systems. *Biol Reprod* 67: 327–333.
36. Iguma LT, Lisauskas SF, Melo EO, Franco MM, Pivato I, et al. (2005) Development of bovine embryos reconstructed by nuclear transfer of transfected and non-transfected adult fibroblast cells. *Genet Mol Res* 4: 55–66.
37. Zakhartchenko V, Mueller S, Alberio R, Scherthauer W, Stojkovic M, et al. (2001) Nuclear transfer in cattle with non-transfected and transfected fetal or cloned transgenic fetal and postnatal fibroblasts. *Mol Reprod Dev* 60: 362–369.
38. Matsunari H, Onodera M, Tada N, Mochizuki H, Karasawa S, et al. (2008) Transgenic-cloned pigs systemically expressing red fluorescent protein, Kusabira-Orange. *Cloning Stem Cells* 10: 313–323.
39. Fujimura T, Murakami H, Kurome M, Takahagi Y, Shigehisa T, et al. (2008) Effects of recloning on the efficiency of production of alpha 1,3-galactosyltransferase knockout pigs. *J Reprod Dev* 54: 58–62.
40. Sternberg N, Hamilton D (1981) Bacteriophage PI site-specific recombination. I. Recombination between loxP sites. *J Mol Biol* 150: 467–486.
41. Whyte JJ, Prather RS (2012) Cell Biology Symposium: Zinc finger nucleases to create custom-designed modifications in the swine (*Sus scrofa*) genome. *J Anim Sci* 90: 1111–1117.
42. Miller JC, Holmes MC, Wang J, Guschin DY, Lee YL, et al. (2007) An improved zinc-finger nuclease architecture for highly specific genome editing. *Nat Biotechnol* 25: 778–785.
43. Szczepk M, Brondani V, Buchel J, Serrano L, Segal DJ, et al. (2007) Structure-based redesign of the dimerization interface reduces the toxicity of zinc-finger nucleases. *Nat Biotechnol* 25: 786–793.
44. Carlson DF, Tan W, Lillico SG, Sverakova D, Proudfoot C, et al. (2012) Efficient TALEN-mediated gene knockout in livestock. *Proc Natl Acad Sci U S A* 109: 17382–17387.

45. Cao X, Shores EW, Hu-Li J, Anver MR, Kelsall BL, et al. (1995) Defective lymphoid development in mice lacking expression of the common cytokine receptor gamma chain. *Immunity* 2: 223–238.
46. DiSanto JP, Muller W, Guy-Grand D, Fischer A, Rajewsky K (1995) Lymphoid development in mice with a targeted deletion of the interleukin 2 receptor gamma chain. *Proc Natl Acad Sci U S A* 92: 377–381.
47. Sugamura K, Asao H, Kondo M, Tanaka N, Ishii N, et al. (1996) The interleukin-2 receptor gamma chain: its role in the multiple cytokine receptor complexes and T cell development in XSCID. *Annu Rev Immunol* 14: 179–205.